Supplementary material to "Appearance and disappearance rates of Phanerozoic marine animal paleocommunities"

A. D. Muscente[1,2*], Rowan C. Martindale[2], Anirudh Prabhu[3], Xiaogang Ma[4], Peter Fox[3], Robert M. Hazen[5], and Andrew H. Knoll[6]

[1]Department of Geology, Cornell College, 600 First Street SW, Mount Vernon, Iowa, 52314, USA

[2]Department of Geological Sciences, The University of Texas at Austin, 1 University Station C1100, Austin, Texas 78712, USA

[3]Department of Earth and Environmental Sciences, Rensselaer Polytechnic Institute, Jonsson-Rowland Science Center, 1W19, 110 8th Street, Troy, NY 12180, USA

[4]Department of Computer Science, University of Idaho, 875 Perimeter Drive, MS 1010, Moscow, Idaho, 83844, USA

[5]Geophysical Laboratory, Carnegie Institution for Science, 5251 Broad Branch Road, Washington, D.C. 20015, USA

[6]Department of Organismic and Evolutionary Biology, Harvard University, 26 Oxford Street, Cambridge, MA 02138, USA

MATERIALS AND METHODS

Data

Our study makes use of global data on collections of animal genera from marine and marginal marine rocks of Phanerozoic age, which were accessed from the Paleobiology Database (PBDB; https://paleobiodb.org/#/) on August 12, 2018 (Alroy, 2003; Peters and McClennen, 2015) using the following link:

http://paleobiodb.org/data1.2/occs/list.csv?datainfo&rowcount&base_name=Animalia&taxon_reso=genus&idqual=genus_certain&pres=regular&interval=Phanerozoic&envtype=marine,marginal,reef,stshallow,stdeep,offshore,slope,marindet&show=full,timebins,acconly

To develop the dataset, we downloaded data on all occurrences of fossils assigned to genera with "accepted names," according to the opinions in the database at the time of data acquisition. The dataset includes cases of fossils identified to the species level as well as fossils that are only assigned to genera. We omitted form and trace fossil taxa and revised the data to correct for synonymous and inconsistently ranked genera (see SI Dataset), leaving 126,174 collections representing 641,923 occurrences of 26,953 valid genera. Overall, the dataset includes the age, formation, state, country, tectonic plate, lithology, environment, and taxonomic richness (genus count) of each collection. We revised the lithology and paleoenvironment data to reduce redundancy (Tables S1, S2), and assigned the collections to time bins (chronostratigraphic stages) using the standard 'major' method, wherein a collection is assigned to a time bin if 50% or more of its regional stratigraphic unit overlaps the chronostratigraphic stage (Muscente et al., 2018; Peters and McClennen, 2015). For some analyses, we also binned the collection using the relatively restrictive "contain" method, where a collection is assigned to a time bin if its regional stratigraphic unit can be correlated with strata located entirely between the upper and lower boundaries of the chronostratigraphic stage (Muscente et al., 2018; Peters and McClennen, 2015).

Network data structure

For the network analysis, we structured the collection data into a unipartite network with weighted connections (Muscente et al., 2018, 2019). The network in this study consists of two basic elements (Fig. S2): nodes (independent entities) and links (connections). Each node (n=124,605) is a fossil collection (Fig. S1), and each link (n=47,294,900) connects two collections that share a simple association of one or more genera. We omitted collections lacking any connections (n=1,323) as well as other collections (n=245) restricted to small, isolated components (i.e., groups of interconnected nodes lacking connections to other nodes in the network), so the data collectively represent 640,015 occurrences of 25,749 total genera, including 21,338 extinct (82.9%) and 3,989 extant (15.5%) taxa (the 422 uncounted taxa, or remaining 1.6%, are probably extinct). The network does not contain multiple edges (i.e., multiple links between nodes) or loops (i.e., links connecting nodes to themselves). We assigned each link a connection strength (weight) related to the taxonomic similarity of its two collections (Shi, 1993), which we calculated from the presence/absence of taxa using binary indices (Shi, 1993). Traditionally, the Jaccard index is favored for multivariate analysis in paleoecology (Shi, 1993). We also assigned weights to the nodes based on their taxonomic richness, so the collections of greatest richness exert the largest effect on network structure.

Network graph

In network graphing (Fig. S2), nodes of equal size were placed at lengths relative to each other according to the Fruchterman-Reingold force-directed algorithm using functions in the igraph package written in the R programming language (Csardi and Nepusz, 2006). The algorithm incorporated the connection weights (equal to the Jaccard similarities of the collections) in its calculations. The connections at the periphery of the graph were truncated to fit all of the nodes in the space.

Assortativity coefficients and homophily

In order to measure homophily, or the tendency of links to connect nodes possessing similar properties, we calculated 'assortativity coefficients' for various nominal and continuous variables (e.g., age, location, environment, lithology, etc.) using functions of the igraph package in RStudio (Csardi and Nepusz, 2006). These coefficients (Table S3) are similar to Pearson correlation coefficients. Values range from 0 to 1; high values reflect a great tendency for similar nodes to be connected, and vice versa.

Community detection algorithms

The nodes and links of the network make up its community structures. In general, community structures consist of units (modules) that appear in network graphs as clusters of densely connected nodes; a network may contain a fractal structure of repeatedly clustered modules. To explore its community structure and identify paleocommunities, we analyzed the network (Fig. S2) with a variety of 'community detection algorithms' (Table S4) using functions of igraph (Csardi and Nepusz, 2006). All of these algorithms partition networks into modules and have been used in other studies to analyze aspects of community paleoecology (Muscente et al., 2018). The algorithms, however, exemplify different approaches to network partitioning (Muscente et al., 2019; Yang et al., 2016). Their results are often compared in terms of modularity (Q), a network property calculated from the fraction of links that connect nodes of the same module minus the corresponding fraction in an equivalent network with a random distribution of links (Clauset et al., 2004). The Q values in this study also take into consideration the weights of the connections (Csardi and Nepusz, 2006). In general, modularity scores vary from 0 to 1, and values >0.3 are considered good indicators of community structure (Clauset et al., 2004).

We concentrate on outputs of the Infomap Algorithm because (a) unlike other methods, it utilizes both link and node weight data; (b) it does not require input on additional parameters, like step size in the walktrap algorithm; and (c) it produced the results with the greatest Q scores and module counts (Tables S4), indicating that it identified the best and smallest modules (see Supplementary Text below). In particular, the Q scores and module counts were highest for connection weights equal to Jaccard coefficients as opposed to values calculated from other indices (Table S5).

The Infomap Algorithm relies on information theoretic principles; it seeks the community structure that minimizes the expected description length of an infinitely long random walk trajectory, where description length is the expected number of bits per node required to encode the path (Rosvall et al., 2010; Rosvall and Bergstrom, 2007). In other words, the algorithm attempts to identify 'neighborhoods' that frequently trap random walkers. Problematically, the Infomap Algorithm is a non-deterministic method (i.e., it may identify different modules in one run versus the next). To address this concern, we applied the algorithm to the network 200 times,

and compared the results produced by these 200 runs using common distance metrics, like the normalized mutual information (NMI), variation of information (VI), and the Rand and adjusted Rand indices (Table S6). We found that the results (e.g., Q and module count) did not significantly vary from one run to the next (see Supplementary Text below).

Genus diversity and turnover proportions

The generic corrected sampled-in-bin (CSIB) number, or gamma diversity (Figs. 1A, 6A), genus extinction proportion, and genus origination proportion of each time bin (geologic stage) was determined from sample-standardized occurrence data with the subsample function of the divDyn package in R using 1000 iterations of the shareholder quorum subsampling (SQS) method at a quorum of 0.7 (Kocsis et al., 2019). The results were adjusted with a sample coverage estimator based on single reference taxa (Alroy, 2010), and are reported as the average values of those iterations along with 95% confidence intervals, as determined from the 97.5^{th} and 2.5^{th} percentiles of the iterations. Proportions of genus origination and genus extinction (Fig. S6E) were calculated for each time bin with the 'second-for-third' substitution algorithm, which simulations indicate provide the most accurate and precise estimates for the origination and extinction rates of taxa (Alroy, 2015). The taxonomic CSIB diversity and turnover proportions are based on all occurrences of marine and marginal marine animal genera of Phanerozoic age in the PBDB, regardless of whether or not the genera occur within the collections included in the unipartite network (Fig. S2).

Paleocommunity diversity and turnover proportions

To explore ecologic change over time, we quantified the diversity and turnover of the modules (paleocommunities) using methods for measuring diversity, origination, and extinction of taxa (Alroy, 2008, 2015). Following traditional methods for measuring taxonomic change, in this approach, we treat the paleocommunities like taxa and collections like occurrences of these 'taxa.' The first appearance datum of a paleocommunity corresponds to its oldest collection(s), and the last appearance datum of a paleocommunity corresponds to its youngest collection(s). The diversity of paleocommunities in a time bin (chronostratigraphic stage) equals their CSIB number (Figs. 1A, S6B), determined using the subsample function of the divDyn package in R (Kocsis et al., 2019). We quantify the appearance and disappearance of communities over time by calculating their proportions of 'origination' (appearance) and 'extinction' (disappearance) for each time bin (i.e., chronostratigraphic stage) in the Phanerozoic (Figs. 2, S6C, D). We calculated these proportions according to the 'second-for-third' rate estimator, which simulations indicate provide the most accurate and precise estimates for origination and extinction of taxa (Alroy, 2015). Prior to calculating the diversity and turnover proportions, we standardized the paleocommunity occurrence data by applying the SQS method to subsample fossil collections. We performed SQS and calculated the CSIB values and turnover proportions using the subsample() function of the divDyn package in R (Kocsis et al., 2019) and a quorum size of 0.8. The procedure involved 1000 iterations and the results were adjusted with a sample coverage estimator based on single collection modules (Alroy, 2010).

Because the Infomap Algorithm is a non-deterministic method (i.e., it may identify different modules in one run versus the next), we applied the algorithm to the network 200 times and derived our best estimates of paleocommunity CSIB diversity and turnover for each run—the 'best estimates' correspond to the average values of diversity and turnover from 1000 iterations of SQS. We report our measures of paleocommunity diversity and turnover as the

average values of those best estimates along with their variation among 200 runs of Infomap. The variation in the results reflect uncertainty created by random chance and probability in the parameters of the Infomap Algorithm.

The number of genera per paleocommunity (alpha diversity) and the number of paleocommunities per genus were calculated from occurrences of taxa and communities that were actually sampled within each bin. Paleocommunity differentiation (beta diversity) equals the average pairwise Jaccard distance (or dissimilarity) between paleocommunities that were sampled within each bin (Shi, 1993). These measures of diversity are based on the complete dataset rather than subsamples, and are reported as the average values and ranges of values from 200 runs of the Infomap algorithm on the network.

Uncertainty in turnover rate calculations

Besides the stochastic uncertainty associated with variation in the results of SQS and the Infomap algorithm, the paleocommunity turnover rate values in this study have a second form of intrinsic uncertainty related to the binomial probabilities of paleocommunities actually appearing and disappearing in the time bins. Consider disappearance rate. All of the paleocommunities within a time bin represent a sample, and the number of paleocommunities equals its sample size. The disappearance rate of the time bin depends on the number of paleocommunities that make their last appearance within the bin (the number of "successes") and the number of paleocommunities that survive until the next bin (the number of "failures"). For a sample of paleocommunities from a time bin with a given turnover rate, it may be observed that fewer or more paleocommunities disappear than expected. The number of "successes" varies from one sample to the next according to the binomial probability distribution, with the observed number approaching the expected number for large sample sizes (i.e., total numbers of paleocommunities).

To account for stochastic and binomial uncertainty, we calculated the errors of the turnover rate values using the following procedure. First, for each run of the Infomap algorithm, we derived our best estimates of the disappearance and appearances rates of the paleocommunities in each time bin using the 'second-for-third' rate estimator (see Paleocommunity diversity and turnover proportions), and then calculated the 95% binomial proportion confidence intervals (CIs) of the values using the normal approximation method based on central limit theorem. Second, for each time bin, we arrayed the upper and lower limits of the 95% CIs calculated in repeated runs of the Infomap algorithm. Lastly, we determined the 97.5^{th} and 2.5^{th} percentile values of the upper and lower limits of disappearance and appearance for each time bin. As a consequence of this procedure, the error bars on the palecommunity turnover rate values in this study illustrate both stochastic and binomial uncertainty.

Correlations

We performed regression analyses in order to assess the direction and strength of the relationship (correlation) between taxonomic and ecologic turnover for the 100 stages in the Phanerozoic record. In these regressions, one variable is taxonomic turnover, defined as genus extinction or origination rate; and the other variable is ecologic change, corresponding to paleocommunity disappearance or appearance rate. Strictly speaking, neither taxonomic turnover nor ecologic change represents an "independent variable;" they are interchangeable. In addition, the measurements of these rates are subject to error, as they are derived from results of repeated subsampling and non-deterministic algorithms. For these reasons, we used the reduced major

axis (RMA) method (also known as Model II) of regression as opposed to ordinary least square (OLS) methods, such as Spearman's rho (ρ), Kendall's tau (τ), and Pearson's r. Unlike the OLS methods (Mukaka, 2012; Schober et al., 2018), the RMA method does not differentiate between "independent" and "dependent" variables, and assumes a pattern of error variance in the data (Smith, 2009). The RMA method, consequently, is generally considered to be the best approach to regression for analyses of bivariate data with measurement error in both variables.

To address any potential issues with distributions of values for the variables, we repeated the regression analyses on two variations of the turnover rate data: (1) the raw second-for-third proportions of the time bins (Figs. S11-S13) and (2) the time bins' ranks with respect to their relative turnover rates (Figs. 3, S7-S10, S13). Notably, the raw second-for-third proportions are not normally distributed and include a number of outliers, in part, due to inclusion of time bins (i.e., mass extinctions) with atypically high rates of taxonomic extinction and community disappearance (Raup and Sepkoski, 1982). To "normalize" the data, we transformed the raw continuous data (i.e., turnover proportions) into ordinal data. The ranks of the time bins have a normal distribution (Figs. 3, S7-S10, S13).

We performed the regression analyses using the "standardized major axis" (SMA) method of the lmodel2 package in R (Legendre, 2018), as SMA is equivalent to RMA in lmodel2. The results of each RMA regression include (1) an equation describing the 'best fit' of the bivariate relationship between two variables; (2) its correlation coefficient (R); (3) the coefficient of determination (i.e., R-squared value); (4) 95% confidence intervals for the y-intercept and slope; and (5) 2- and 1-tailed parametric p-values. Correlations with p-values less than alpha (0.05) are considered statistically significant.

Data standardization and sensitivity analyses

To confirm that ecologic change is positively correlated with taxonomic change and that our results are robust, we standardized the data and conducted sensitivity analyses to address four potential types of error (Muscente et al., 2019): (a) unequal sampling of fossil collections affecting diversity and proportion calculations; (b) unequal sampling of fossil collections affecting identification of paleocommunities; (c) autocorrelation between taxonomic and ecologic turnover caused by similar term trends in the time series; and (d) correlation between taxonomic and ecologic turnover caused by the inclusion of low diversity collections and modules in the analyses.

Unequal sampling of fossils of various ages may introduce errors into diversity and turnover proportion calculations (Alroy, 2003, 2008). To minimize these errors, prior to calculating the paleocommunity CSIB numbers and turnover proportions, we standardized the paleocommunity occurrence data by applying the SQS method with the subsample() function of the divDyn package in R (Kocsis et al., 2019) and a quorum of 0.8. The procedure involved 1000 iterations and the results were adjusted with a sample coverage estimator based on single collection modules (Alroy, 2010).

Given that stratigraphic position exerts a strong control on network topology, unequal sampling of collections of different ages may also affect module (i.e., paleocommunity) identification. We investigated this possibility by repeatedly subsampling a given number of collections from each chronostratigraphic system, equal to the duration of the period multiplied by the number of collections per million years in the Cambrian, the oldest and least sampled period (94.67 collections/million years). In total, we produced 100 subsamples, each of 51,216 collections. From each subsample, we produced a subnetwork (Muscente et al., 2019). As

community detection algorithms tend to identify each component of a multi-component network as a module, we omitted collections lacking any connections as well as others belonging to isolated components (i.e., groups of interconnected nodes lacking connections to other nodes in the largest component); therefore, instead of 51,216 collections, each subnetwork consisted, on average, of 50,589 nodes (minimum: 50,472; maximum 50,664). In other words, each subnetwork is roughly 41% (50,589/124,605) of the whole (original) network. To each subnetwork, we applied the Infomap Algorithm, and compared its results to a random clustering of the whole network by calculating common distance metrics for comparing community structures, like NMI, VI, and the Rand and adjusted Rand indices (Table S8). For each calculation, we only considered collections found in the whole network and subnetwork (i.e., collections in the whole network, but absent in the subnetwork, did not factor into calculation).

When time series follow similar long-term trends, they may be correlated, even though the direct relationships among the data are weak. To confirm that the results do not reflect this autocorrelation, we subjected the raw data (ecologic and taxonomic turnover proportions and ranks) to first-differencing, calculating first-differenced data points, each representing the difference between two consecutive time bins for a given turnover metric. We then repeated the regression analyses using the first-differenced data. Correlations between time series subjected to first differencing are considered robust to autocorrelation (Fig. S13).

Additional errors may originate from the inclusion of low diversity collections and modules (i.e., those with few genera) in the proportion calculations. Some of these collections and modules may represent low diversity (e.g., monospecific) communities or they may be artefacts of incomplete sampling or data entry. In any case, low diversity collections may be poor markers of their modules if they consist of taxa that occur in multiple paleocommunities, and the appearance and disappearance of low diversity modules will tend to mirror the origination and extinction of taxa, as the effects of adding or subtracting a taxon are amplified at lower diversity levels. To address these concerns, we adopted a thresholding approach, systematically excluding collections and modules of varying diversity level from the proportion calculations, and for each run at a combination of thresholds, recalculating the regression statistics for the correlation between taxonomic and ecologic change. The results are presented as Kendall rank correlation (τ) coefficients (Fig. S14). We calculated τ for the turnover of the subsampled paleocommunities and all of the collections in network (Fig. S14A, S14B). In addition, we calculated the correlation between the proportions of the subsampled paleocommunities and all of the genera in the Phanerozoic (Fig. S14C, S14D). For this work, prior to calculating the paleocommunity turnover proportions, we standardized the subsampled paleocommunity occurrence data using the SQS method using the subsample() function of the divDyn package in R (Kocsis et al., 2019). As more and more collections were omitted, it was necessary to increase the quorum size of the SQS method in order to ensure there was sufficient coverage, but in each instance, the smallest quorum size (generally between 0.7 and 0.9) was used. Each SQS analysis involved 100 iterations and the results were adjusted with a sample coverage estimator based on single collection modules (Alroy, 2010).

SUPPLEMENTARY RESULTS

Additional description of collections and modules in the network

Most collections in the network (51%) contain three or more animal genera (Fig. S3A). Although the distributions are positively skewed, most of the modules (54%) have been sampled eight or more times (Fig. S3B) and represent four or more genera (Fig. S3C). Indeed, the number

of genera per module is positively correlated with the number of collections per module (Adjusted R-squared value = 0.71), and the correlation is statistically significant (p-value < 0.001) for both linear and multiple linear regression models (Fig. S4). This relationship is a consequence of the classic relationship between sampling and diversity, as more samples (collection) translates into more taxa, everything else being equal.

When applied to the unipartite network in this study, the Infomap Algorithm returned the highest module counts and Q scores of all the community detection algorithms (Yang et al., 2016), indicating that it performed best at identifying modules (Muscente et al., 2018, 2019), specifically when connection weight equals the Jaccard similarity of collections (Tables S4, S5). When we repeatedly applied the Infomap Algorithm to the unipartite network, we found that the results (e.g., Q and module count) did not significantly vary from one run to the next. With the Jaccard index, the algorithm returned, on average, 3937 modules with a Q of 0.85. The NMI values, which are commonly used to compare community structures (Karrer et al., 2008; Muscente et al., 2019), show that two successive random runs of the algorithm typically differ by only 1% of their information (Table S6).

The majority of modules are limited to two or fewer lithologies, paleoenvironments, states, countries, and tectonic plates (Fig. S5). Most modules (69%) are limited to a single chronostratigraphic system (Fig. S5H); however, the majority (55%) have been sampled in two or more chronostratigraphic stages (Fig. S5I, S5K). If one accounts for sampling gaps between the oldest and youngest collections assigned to each module, the majority (55%) of modules represent time intervals spanning three or more ages, each on average, about 5-10 million years in duration (Fig. S5L). Random forest analysis (Breiman, 2001) indicates that tectonic plate is the best explanatory variable for module assignment followed by paleoenvironment (our revisions), lithology (our revisions), and system (Table S7). Given these results, we interpret the modules as paleocommunities for the following reasons: (1) the fossil collections are samples of local paleocommunities, (2) the collections in each module cannot be distinguished by methods that return the best Q values, and (3) most modules span narrow environmental and geographic ranges, even though they existed in one form or another for tens of millions of years.

Results from standardization and sensitivity analyses

The correlations between ecologic and taxonomic turnover are robust to the four types of error considered in this study. They are robust to unequal sampling of fossil collections from different systems. When we applied the Infomap Algorithm to standardized subnetworks, each with about 50,589 collections/nodes (~41% of the nodes in the whole network), we found that the community structures were generally similar to those produced from analysis of the whole network, both in term of modularity score (average Q = 0.85) and the actual module assignments of the collections (Table S8). The NMI scores comparing the whole network to the subnetwork clusterings show that they generally differ, on average, by about 5% of their information, even though the subnetworks contained 59% fewer collections. Second, the results do not change when the data are subjected to first-differencing; we still find a significant correlation between taxonomic and ecologic turnover (Fig. S13). Lastly, exclusion of low diversity collections (≤7 genera) and modules (≤25 genera) does not alter the turnover proportions or time bin ranks (Fig. S14A, S14B); we find a significant correlation between taxonomic and ecologic change, even if 75% of the collections are omitted prior to calculation of the ecologic turnover proportions and time bin ranks (Fig. S14C, S14D). In summation, none of the standardization and sensitivity analyses alter the outcomes of the study.

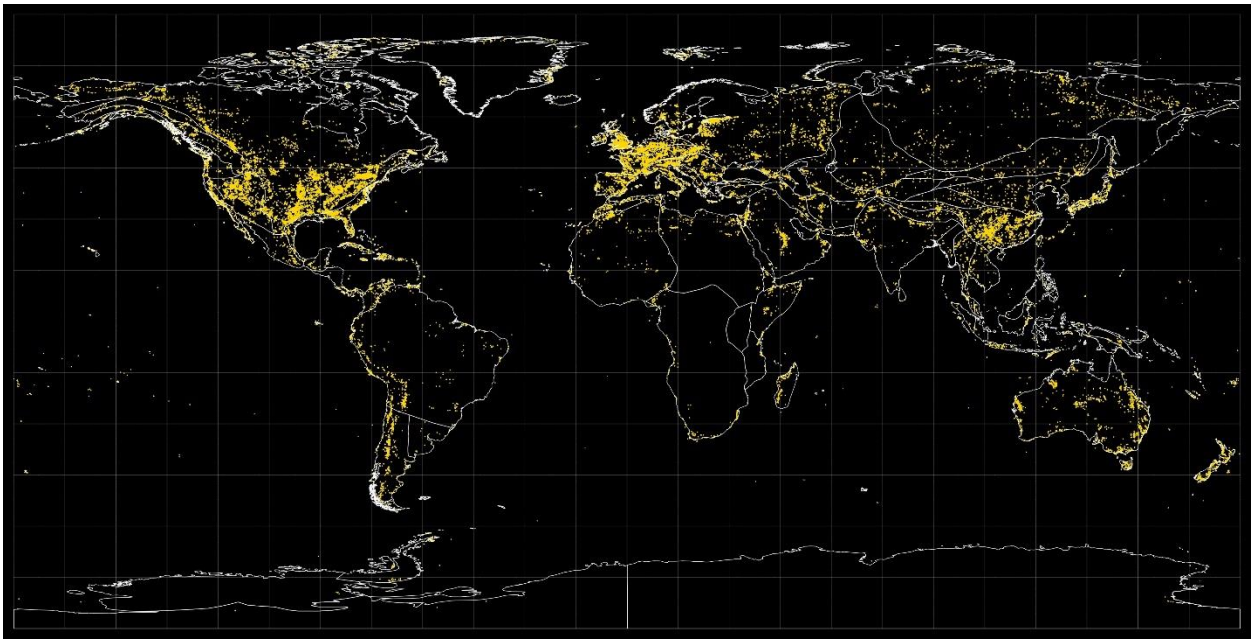

Figure S1. Global map of fossil collections (yellow dots) that make up the network in this study. All data on collections (n=124,599) were accessed from the Paleobiology Database (PBDB), specifically the ‘lat’ (latitude) and ‘lng’ (longitude) fields. Six of the collections in the network do not have latitudinal and/or longitudinal coordinates, and therefore, are not shown in the map.

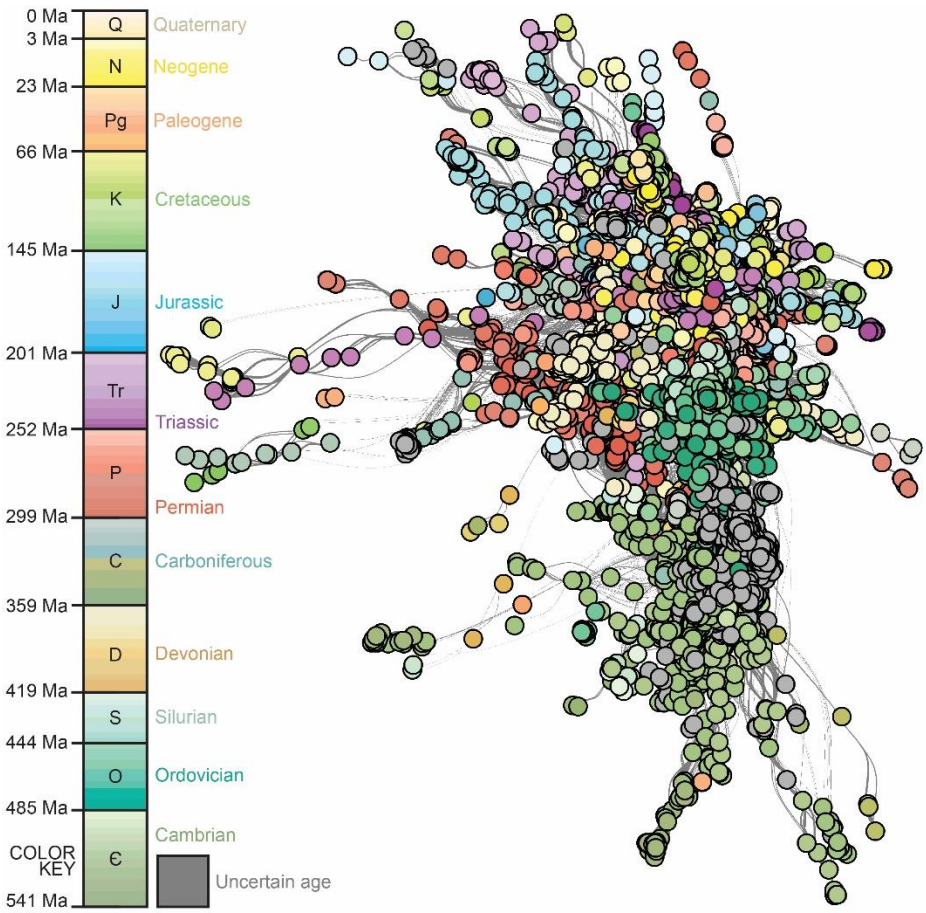

Figure S2. Graph of the unipartite network. Each node is a fossil collection, and two nodes are connected if they share one or more marine or marginal marine animal genera. Node weight (not illustrated) equals the number of genera in the collection, and connection weight equals the Jaccard similarity of the collections. The color of each collection indicates its time bin (chronostratigraphic stage) as shown in the geologic column with absolute ages provided in *Mega anna* (Ma).

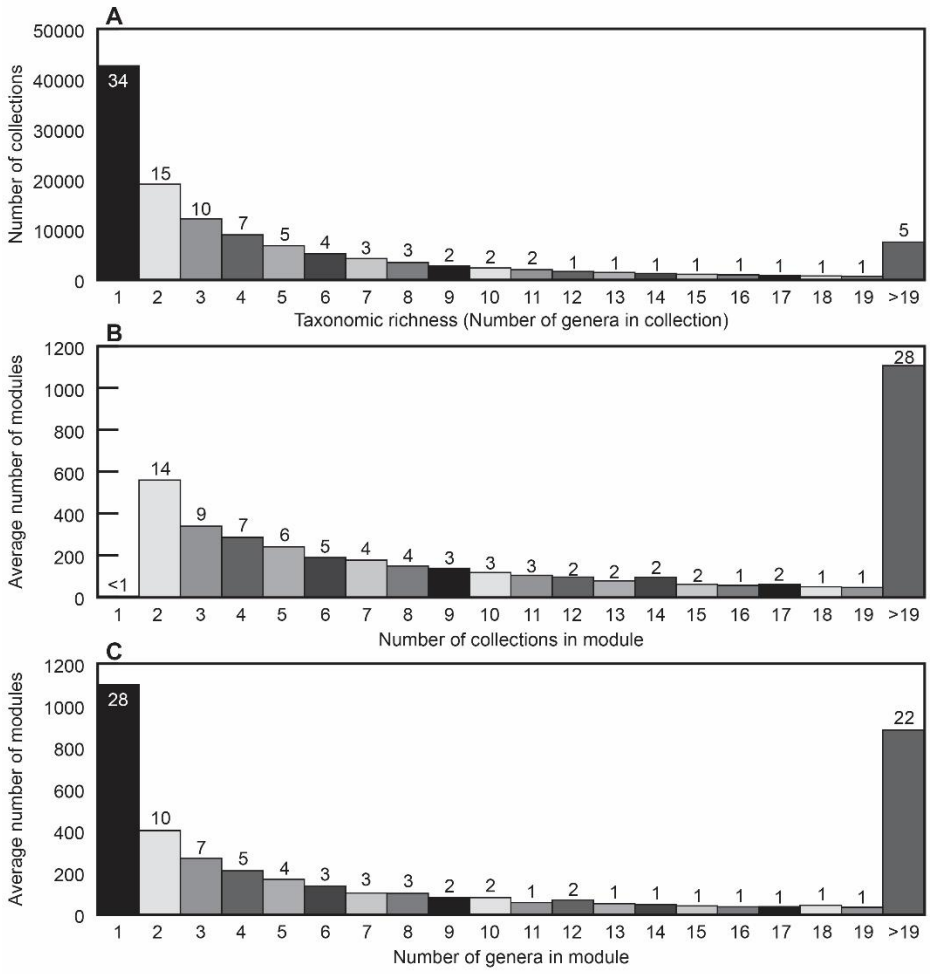

Figure S3. Bar plots describing collections and modules in the network. A: Number of collections versus taxonomic richness (number of genera) of each collection. B: Number of modules versus the number of collections in each module. C: Number of modules versus the number of genera represented by each module. The values represented by the y-axes in (B, C) are averages from 200 runs of the Infomap Algorithm on the network (Fig. S2).

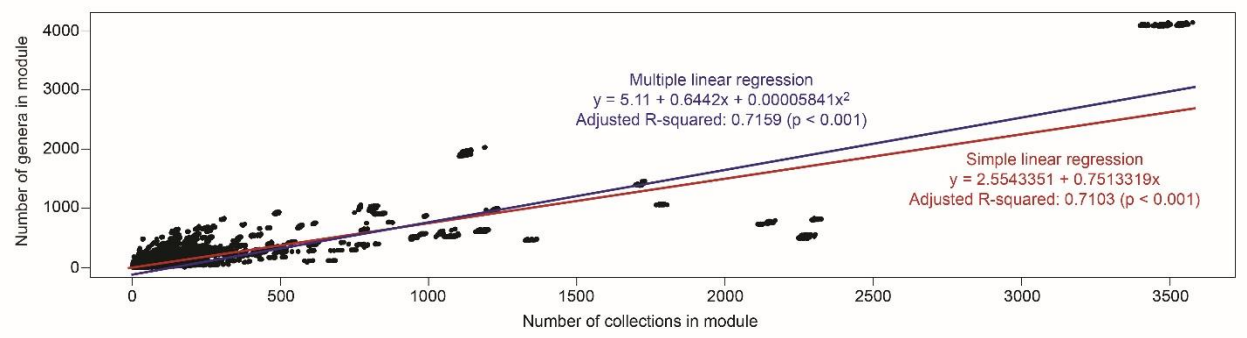

Figure S4. Regression of the numbers of genera and collections in each module of the network. Each data point represents a module identified in one of 200 runs of the Infomap Algorithm on the network (Fig. S2). The x-axis is the number of collections assigned to the module, and the y-axis is the number of genera represented by the collections in the module. The red and blue lines illustrate the results of linear and multiple linear regression analyses, respectively. These results include adjusted R-squared and associated p values. Correlations with p values less than alpha (0.05) are statistically significant.

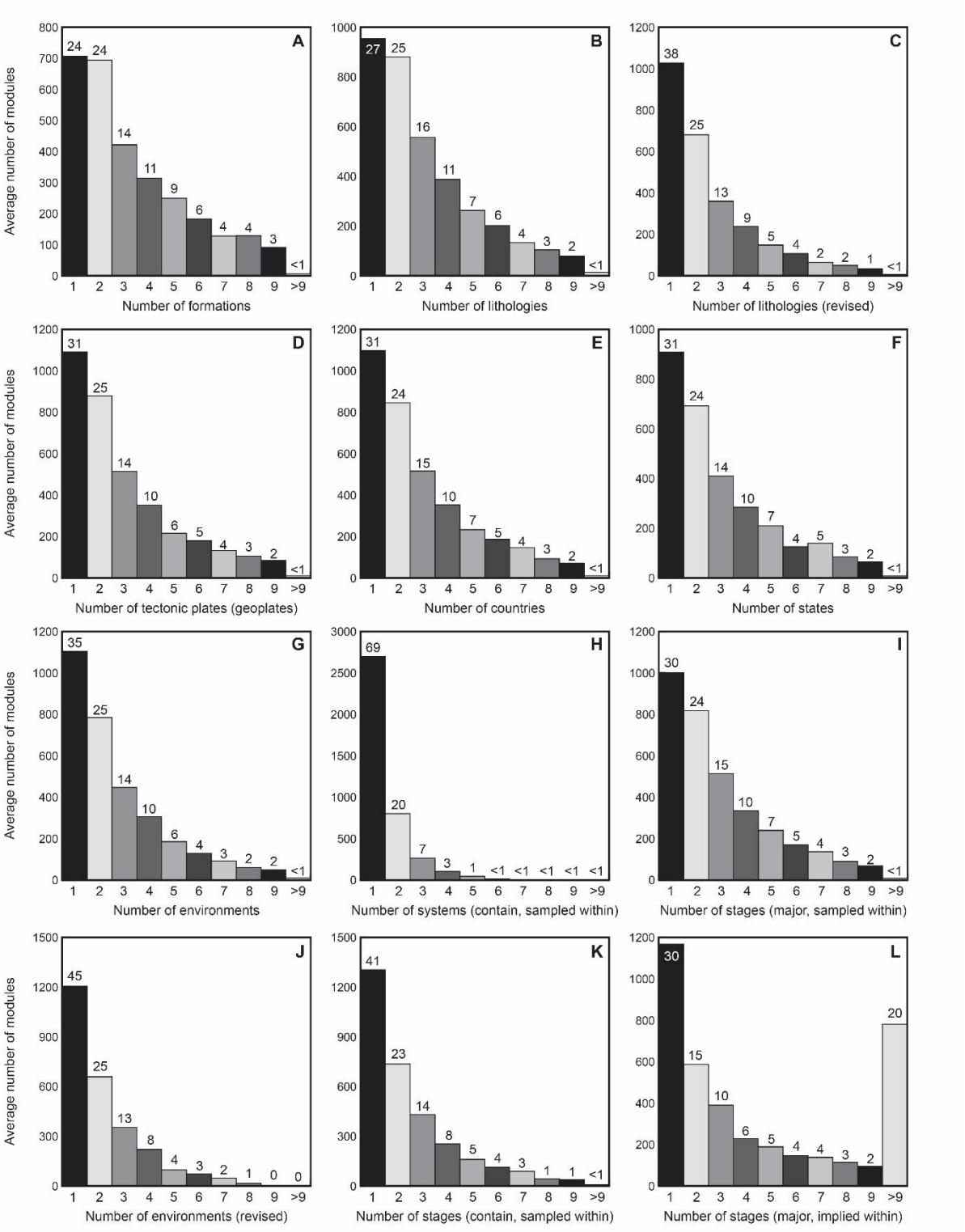
A
Average number of modules
Number of formations
B
Number of lithologies
C
Number of lithologies (revised)
D
Number of tectonic plates (geoplates)
E
Number of countries
F
Number of states
G
Number of environments
H
Number of systems (contain, sampled within)
I
Number of stages (major, sampled within)
J
Number of environments (revised)
K
Number of stages (contain, sampled within)
L
Number of stages (major, implied within)

Figure S5. Additional bar plots describing modules in the network. For all plots, the y-axis is the average number of modules from 200 runs of the Infomap Algorithm on the network (Fig. S2). Each x-axis is the number of categories (pertaining to a nominal variable) represented by the collections of the individual modules A: formation. B: lithology ('lithology1' field in PBDB). C: revised lithology (data from 'lithology1' field of the PBDB but modified to reduce redundancy; see Table S2). D: tectonic plate ('geoplate' field in PBDB). E: country ('cc' field in PBDB). F: state ('state' field in PBDB). G: environment ('environment' field in PBDB). H: system (collections binned into chronostratigraphic systems using 'contain' method). I: stage ('time_major' field in PBDB; collections binned into chronostratigraphic stages using 'major' method). J: environment (data from 'environment' field of PBDB but modified to reduce redundancy). K: stage ('time_contain' field in PBDB; collections binned into chronostratigraphic stages using 'contain' method). L: stage (modules assigned to all time bins—chronostratigraphic stages—between their oldest and youngest collections).

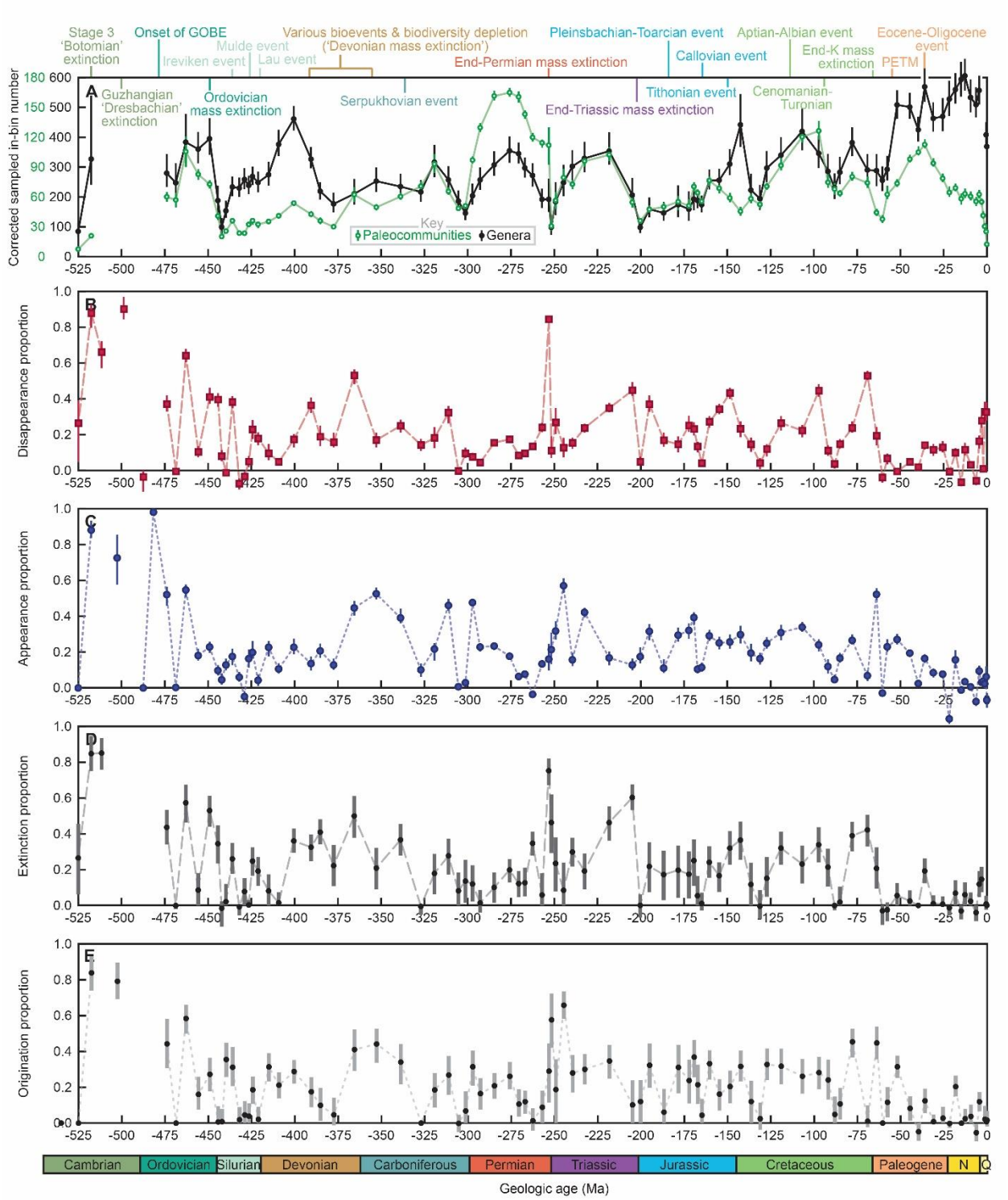
Stage 3 'Botomian' extinction
Onset of GOBE
Various bioevents & biodiversity depletion ('Devonian mass extinction')
Pleinsbachian-Toarcian event
Aptian-Albian event
Eocene-Oligocene event
Mulde event
Ireviken event
Lau event
End-Permian mass extinction
Callovian event
End-K mass extinction
PETM
Guzhangian 'Dresbachian' extinction
Ordovician mass extinction
Serpukhovian event
Tithonian event
End-Triassic mass extinction
Cenomanian-Turonian
Corrected sampled in-bin number
A
Key
Paleocommunities
Genera
B
Disappearance proportion
C
Appearance proportion
D
Extinction proportion
E
Origination proportion
Cambrian
Ordovician
Silurian
Devonian
Carboniferous
Permian
Triassic
Jurassic
Cretaceous
Paleogene
N
Q
Geologic age (Ma)

Figure S6. Line graphs showing the geologic history of ecologic and taxonomic change. A: Corrected sampled-in-bin (CSIB) numbers (Alroy, 2008) of all valid marine and marginal marine animal genera in the PBDB (n = 26,953) and paleocommunities identified by the Infomap Algorithm (Fig. S2) in this study. The so-called 'big five' mass extinctions (Raup and Sepkoski, 1982) and other major biodiversity crises and ecologic transitions in Earth history (Bond and Grasby, 2017; McGhee et al., 2013) are also shown. Generic diversity was determined from sample-standardized occurrence data in the PBDB using the SQS method at a quorum of 0.7, and the results were adjusted with a sample coverage estimator based on single reference taxa (Alroy, 2010). The gaps are consequences of insufficient data. B: The disappearance ('extinction') proportion of paleocommunities. C: The appearance ('origination') proportion of paleocommunities. D: The extinction proportion of marine and marginal animal genera. E. The origination proportion of marine and marginal marine animal genera. The proportions in B-E were calculated with the 'second-for-third' substitution algorithm (Alroy, 2015). The y-axis values of the paleocommunity data in A-C are averages of the best estimates from 200 runs of the Infomap Algorithm, and the error bars illustrate the minimum and maximum values of those runs (i.e., the stochastic uncertainty).

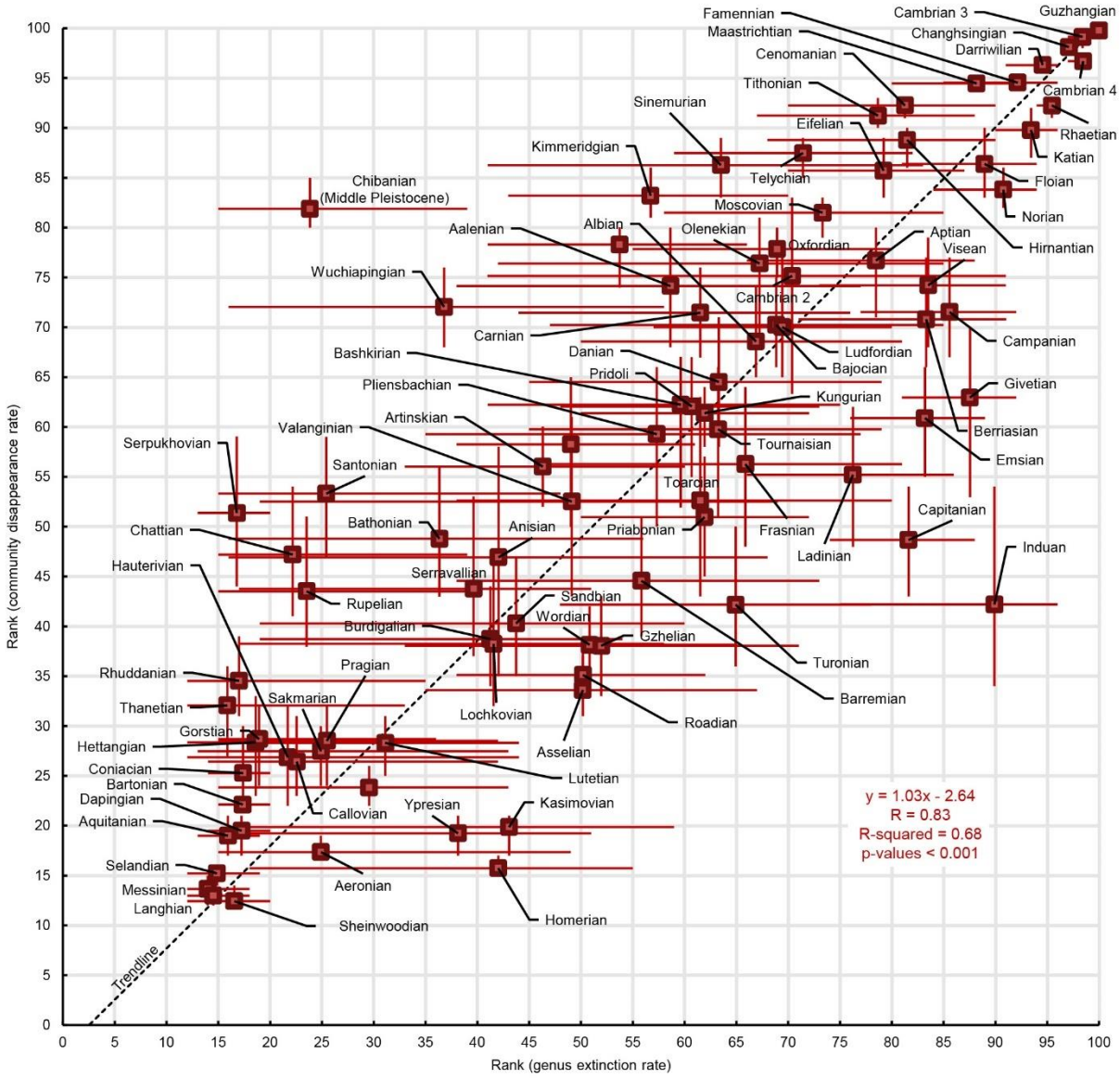

Figure S7. Rank correlation of the proportions of taxonomic extinction and paleocommunity disappearance. The data are the same as those in Fig. 3A, but the plot is enlarged and the data points are labelled. Each point is a time bin (n=89); 11 chronostratigraphic stages were omitted for insufficient data. The axes are the time bins' ranks in terms of their turnover proportions (e.g., Figs. 2, S6C-E), in this case, the extinction proportion of marine and marginal marine animal genera (x-axis) and the disappearance proportion of paleocommunities (y-axis). The plot includes a trendline from reduced major axis regression; coefficient of correlation (R value); coefficient of determination (R-squared value); and associated p-values. The y-axis values are averages of best estimates from 200 runs of Infomap; and the x-axis values are averages from 1000 subsamples of SQS. Error bars illustrate 95% CIs of the values.

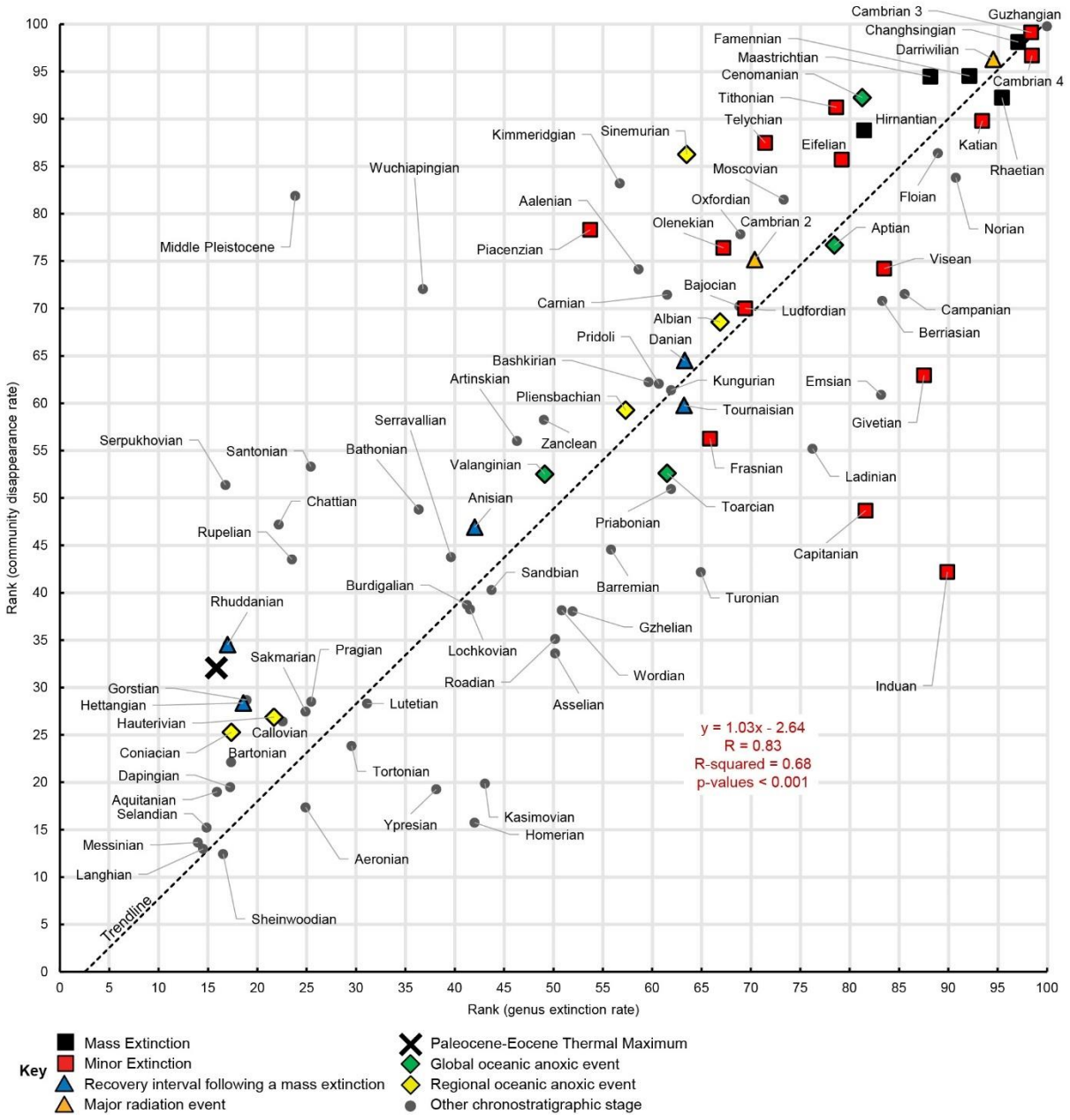
Rank (community disappearance rate)
Rank (genus extinction rate)
Cambrian 3
Guzhangian
Changhsingian
Famennian
Darriwilian
Maastrichtian
Cambrian 4
Cenomanian
Tithonian
Hirnantian
Telychian
Kimmeridgian
Sinemurian
Eifelian
Katian
Wuchiapingian
Moscovian
Rhaetian
Floian
Aalenian
Oxfordian
Norian
Olenekian
Cambrian 2
Middle Pleistocene
Piacenzian
Aptian
Visean
Bajocian
Carnian
Ludfordian
Campanian
Albian
Berriasian
Pridoli
Danian
Bashkirian
Kungurian
Emsian
Artinskian
Pliensbachian
Tournaisian
Givetian
Serravallian
Zanclean
Serpukhovian
Santonian
Bathonian
Frasnian
Ladinian
Valanginian
Chattian
Anisian
Toarcian
Rupelian
Priabonian
Capitanian
Sandbian
Burdigalian
Barremian
Turonian
Rhuddanian
Gzhelian
Sakmarian
Pragian
Lochkovian
Wordian
Gorstian
Roadian
Induan
Hettangian
Lutetian
Asselian
Hauterivian
Callovian
Coniacian
Bartonian
Tortonian
Dapingian
Aquitanian
Selandian
Ypresian
Kasimovian
Homerian
Messinian
Aeronian
Langhian
Sheinwoodian
Trendline
y = 1.03x - 2.64
R = 0.83
R-squared = 0.68
p-values < 0.001
Key
Mass Extinction
Minor Extinction
Recovery interval following a mass extinction
Major radiation event
Paleocene-Eocene Thermal Maximum
Global oceanic anoxic event
Regional oceanic anoxic event
Other chronostratigraphic stage

Figure S8. Ranks of major events in Earth history in terms of the proportions of taxonomic extinction and paleocommunity disappearance. The data are the same as those in Fig. 3A and Fig. S7. Each point is a time bin (n=89); 11 chronostratigraphic stages were omitted for insufficient data. Shapes correspond to different types of events in the stages, including mass extinctions (Bambach, 2006; Bond and Grasby, 2017; McGhee et al., 2013; Sepkoski, 1982), minor extinctions (Bambach, 2006; Bond and Grasby, 2017; McGhee et al., 2013; Sepkoski, 1982), post-mass extinction recovery intervals (Sheehan, 1996), global Oceanic Anoxic Events (Takashima et al., 2006), regional Oceanic Anoxic Events (Takashima et al., 2006), the Paleocene-Eocene Thermal Maximum (Foster et al., 2020; Speijer et al., 2012), and radiations of life like the Cambrian Explosion (Kouchinsky et al., 2012; Landing et al., 2013) and Great Ordovician Biodiversification Event (Servais and Harper, 2018; Servais et al., 2008; Webby, 2004). For this work, we assume that the Induan and Olenekian represent minor extinction event stages and recovery from the Permian-Triassic mass extinction largely occurred in the Anisian, as suggested by various works (Bowring et al., 1999; Chen and Benton, 2012; Foster et al., 2017). We assign the late Mississippian extinction event (the 'Serpukhovian Extinction'), which occurred sometime during the late Visean or early Serpukhovian, to the Visean stage (Balseiro and Powell, 2019; McGhee et al., 2012; Powell, 2008). The axes are the time bins' ranks in terms of their turnover proportions (e.g., Figs. 2, S6C-E), in this case, the extinction proportion of marine and marginal marine animal genera (x-axis) and the disappearance proportion of paleocommunities (y-axis). The plot includes a trendline from reduced major axis regression; coefficient of correlation (R value); coefficient of determination (R-squared value); and associated p-values. The y-axis values are averages of best estimates from 200 runs of Infomap; and the x-axis values are averages from 1000 subsamples of SQS.

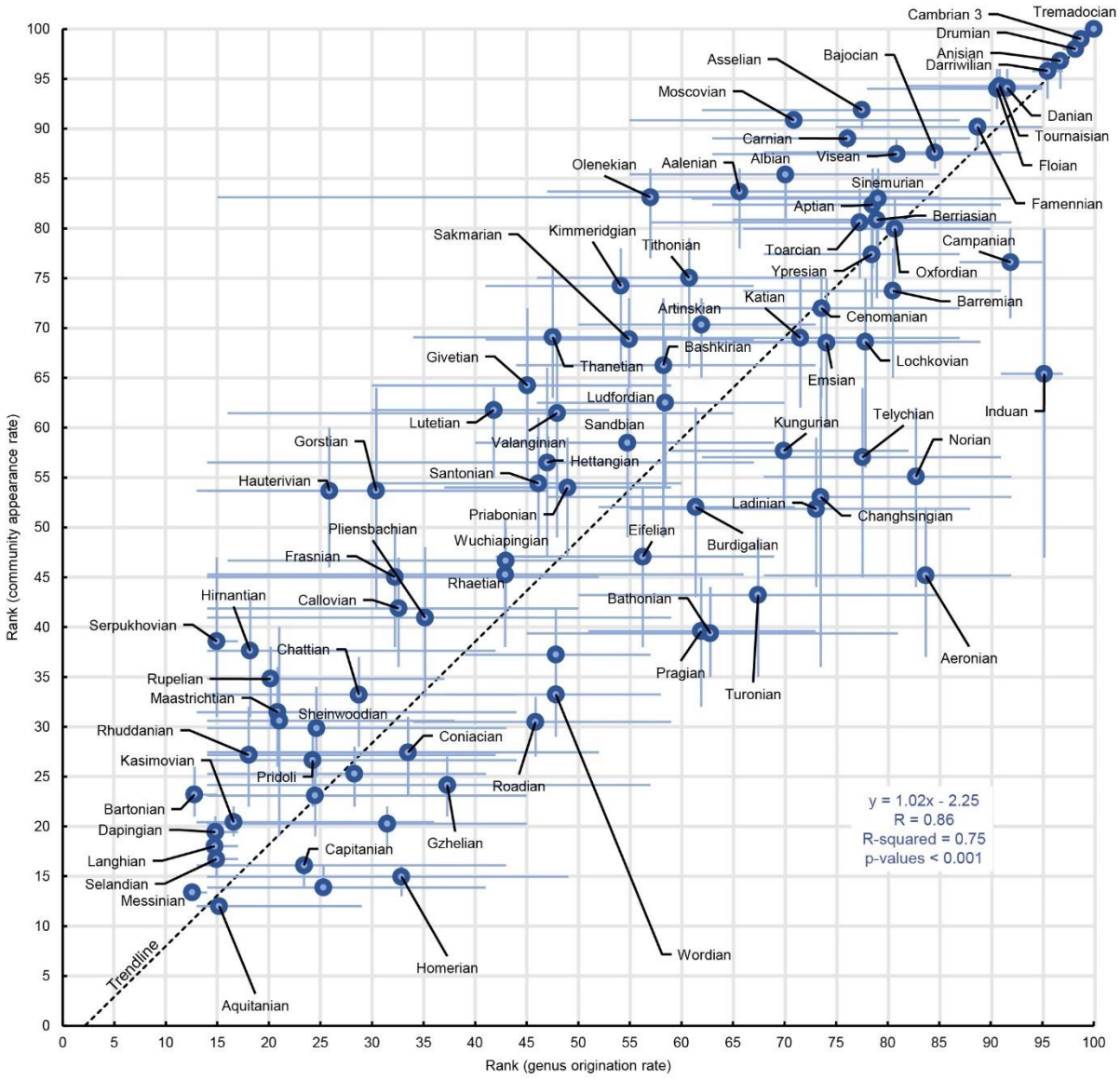

Figure S9. Rank correlation of the proportions of taxonomic origination and paleocommunity appearance. The data are the same as those in Fig. 3B, but the plot is enlarged and the data points are labelled. Each point is a time bin (n=89); 11 chronostratigraphic stages were omitted for insufficient data. The axes are the time bins' ranks in terms of their turnover proportions (e.g., Figs. 2, S6C-E), in this case, the origination proportion of marine and marginal marine animal genera (x-axis) and the appearance proportion of paleocommunities (y-axis). The plot includes a trendline from reduced major axis regression; coefficient of correlation (R value); coefficient of determination (R-squared value); and associated p-values. The y-axis values are averages of best estimates from 200 runs of Infomap; and the x-axis values are averages from 1000 subsamples of SQS. Error bars illustrate 95% CIs of the values.

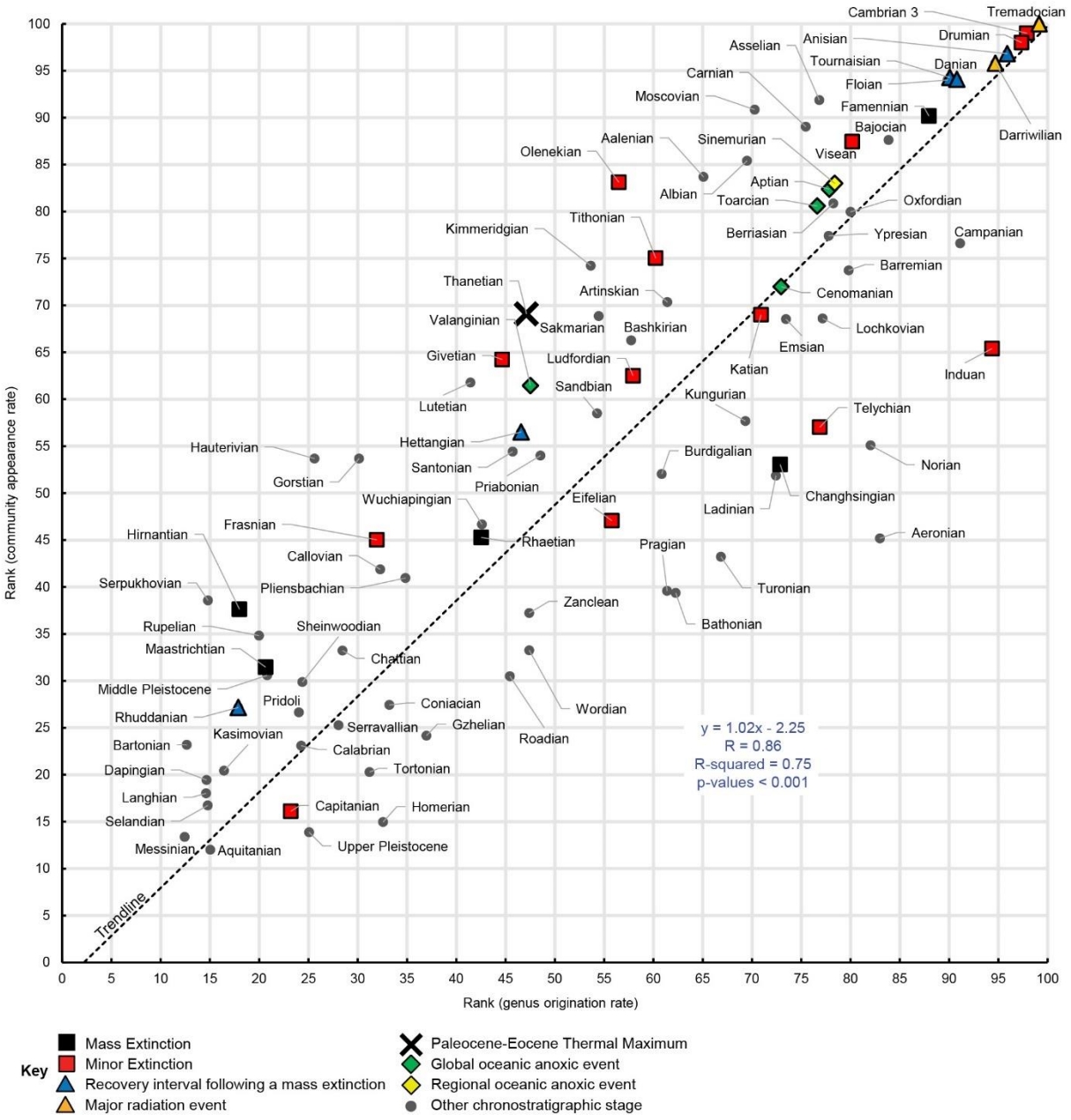
Rank (community appearance rate)
Rank (genus origination rate)
Trendline
y = 1.02x - 2.25
R = 0.86
R-squared = 0.75
p-values < 0.001
Cambrian 3
Tremadocian
Drumian
Anisian
Asselian
Tournaisian
Danian
Carnian
Floian
Moscovian
Famennian
Bajocian
Darriwilian
Aalenian
Sinemurian
Visean
Olenekian
Aptian
Albian
Toarcian
Oxfordian
Tithonian
Berriasian
Ypresian
Campanian
Kimmeridgian
Barremian
Thanetian
Cenomanian
Artinskian
Valanginian
Sakmarian
Bashkirian
Lochkovian
Emsian
Givetian
Ludfordian
Katian
Induan
Sandbian
Lutetian
Kungurian
Telychian
Hettangian
Hauterivian
Burdigalian
Norian
Santonian
Gorstian
Priabonian
Changhsingian
Wuchiapingian
Eifelian
Ladinian
Hirnantian
Frasnian
Rhaetian
Aeronian
Callovian
Pragian
Serpukhovian
Pliensbachian
Turonian
Zanclean
Rupelian
Sheinwoodian
Bathonian
Maastrichtian
Chattian
Middle Pleistocene
Pridoli
Coniacian
Wordian
Rhuddanian
Serravallian
Gzhelian
Kasimovian
Roadian
Bartonian
Calabrian
Dapingian
Tortonian
Langhian
Capitanian
Homerian
Selandian
Messinian
Aquitanian
Upper Pleistocene
Key
Mass Extinction
Minor Extinction
Recovery interval following a mass extinction
Major radiation event
Paleocene-Eocene Thermal Maximum
Global oceanic anoxic event
Regional oceanic anoxic event
Other chronostratigraphic stage

Figure S10. Ranks of major events in Earth history in terms of the proportions of taxonomic origination and paleocommunity appearance. The data are the same as those in Fig. 3B and Fig. S9. Each point is a time bin (n=89); 11 chronostratigraphic stages were omitted for insufficient data. Shapes correspond to different types of events in the stages, including mass extinctions (Bambach, 2006; Bond and Grasby, 2017; McGhee et al., 2013; Sepkoski, 1982), minor extinctions (Bambach, 2006; Bond and Grasby, 2017; McGhee et al., 2013; Sepkoski, 1982), post-mass extinction recovery intervals (Sheehan, 1996), global Oceanic Anoxic Events (Takashima et al., 2006), regional Oceanic Anoxic Events (Takashima et al., 2006), the Paleocene-Eocene Thermal Maximum (Foster et al., 2020; Speijer et al., 2012), and radiations of life like the Cambrian Explosion (Kouchinsky et al., 2012; Landing et al., 2013) and Great Ordovician Biodiversification Event (Servais and Harper, 2018; Servais et al., 2008; Webby, 2004). For this work, we assume that the Induan and Olenekian represent minor extinction event stages and recovery from the Permian-Triassic mass extinction largely occurred in the Anisian, as suggested by various works (Bowring et al., 1999; Chen and Benton, 2012; Foster et al., 2017). We assign the late Mississippian extinction event (the 'Serpukhovian Extinction'), which occurred sometime during the late Visean or early Serpukhovian, to the Visean stage (Balseiro and Powell, 2019; McGhee et al., 2012; Powell, 2008). The axes are the time bins' ranks in terms of their turnover proportions (e.g., Figs. 2, S6C-E), in this case, the origination proportion of marine and marginal marine animal genera (x-axis) and the appearance proportion of paleocommunities (y-axis). The plot includes a trendline from reduced major axis regression; coefficient of correlation (R value); coefficient of determination (R-squared value); and associated p-values. The y-axis values are averages of best estimates from 200 runs of Infomap; and the x-axis values are averages from 1000 subsamples of SQS.

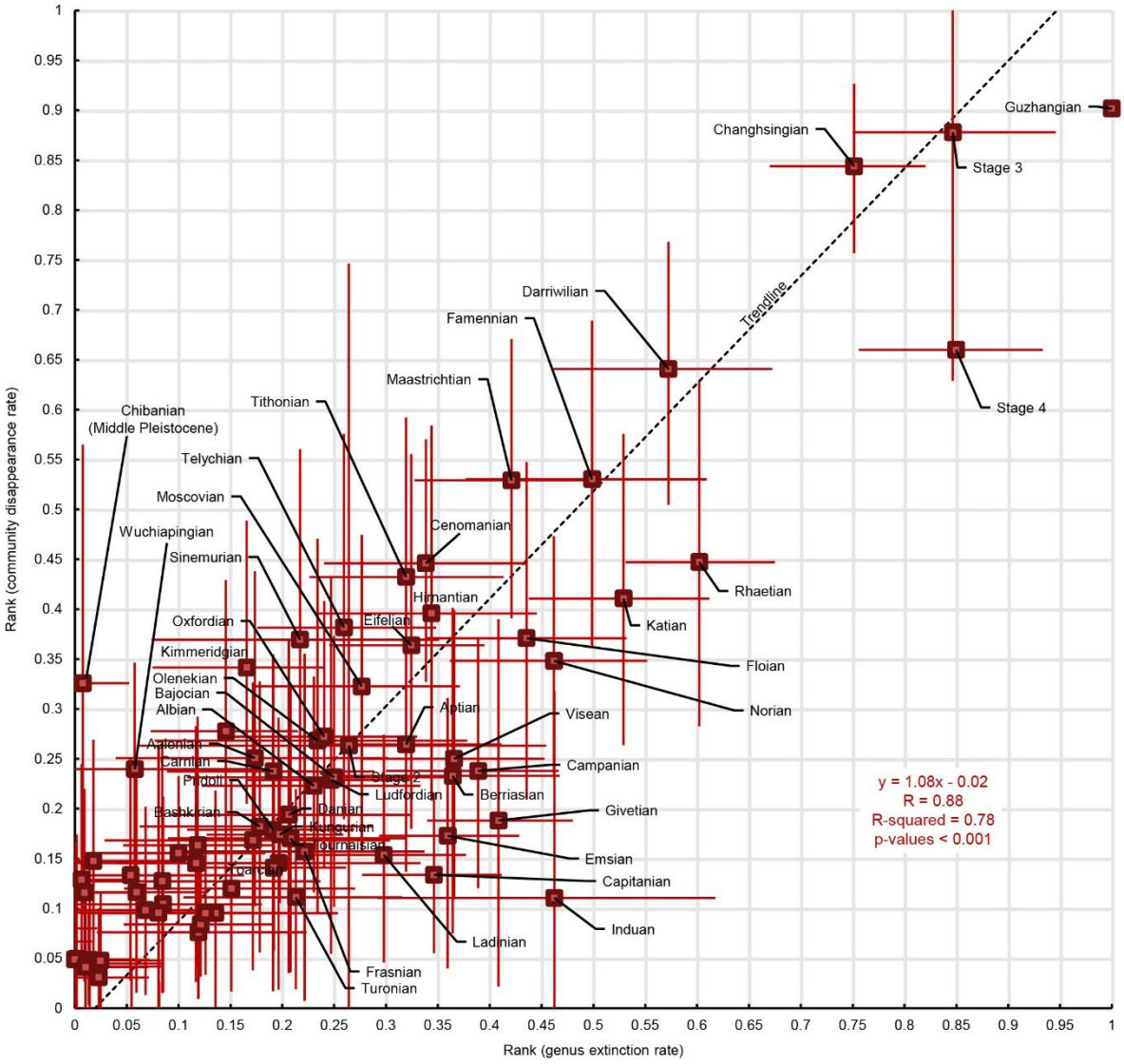

Figure S11. Simple correlation of the proportions of taxonomic extinction and paleocommunity disappearance. Each point is a time bin (n=89); 11 chronostratigraphic stages were omitted for insufficient data. The axes are turnover proportions (e.g., Figs. 3, S6C-E), in this case, the extinction proportion of marine and marginal marine animal genera (x-axis) and the disappearance proportion of paleocommunities (y-axis). The plot includes a trendline from reduced major axis regression; coefficient of correlation (R value); coefficient of determination (R-squared value); and associated p-values. The y-axis values are averages of best estimates from 200 runs of Infomap; and the x-axis values are averages from 1000 subsamples of SQS. Error bars illustrate 95% CIs of the values.

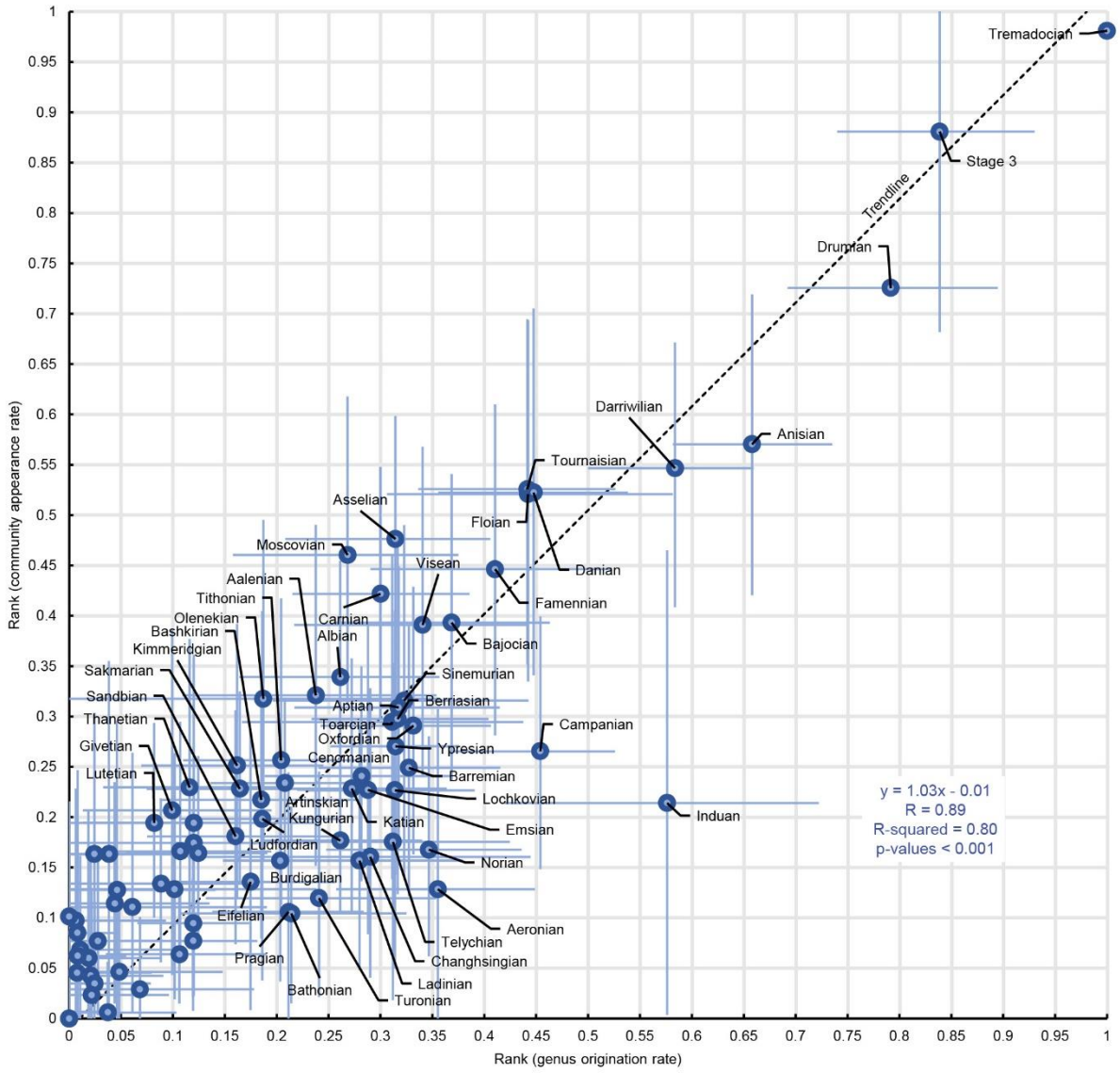

Figure S12. Simple correlation of the proportions of taxonomic origination and paleocommunity appearance. Each point is a time bin (n=89); 11 chronostratigraphic stages were omitted for insufficient data. The axes are turnover proportions (e.g., Figs. 2, S6C-E), in this case, the origination proportion of marine and marginal marine animal genera (x-axis) and the appearance proportion of paleocommunities (y-axis). The plot includes a trendline from reduced major axis regression; coefficient of correlation (R value); coefficient of determination (R-squared value); and associated p-values. The y-axis values are averages of best estimates from 200 runs of Infomap; and the x-axis values are averages from 1000 subsamples of SQS. Error bars illustrate 95% CIs of the values.

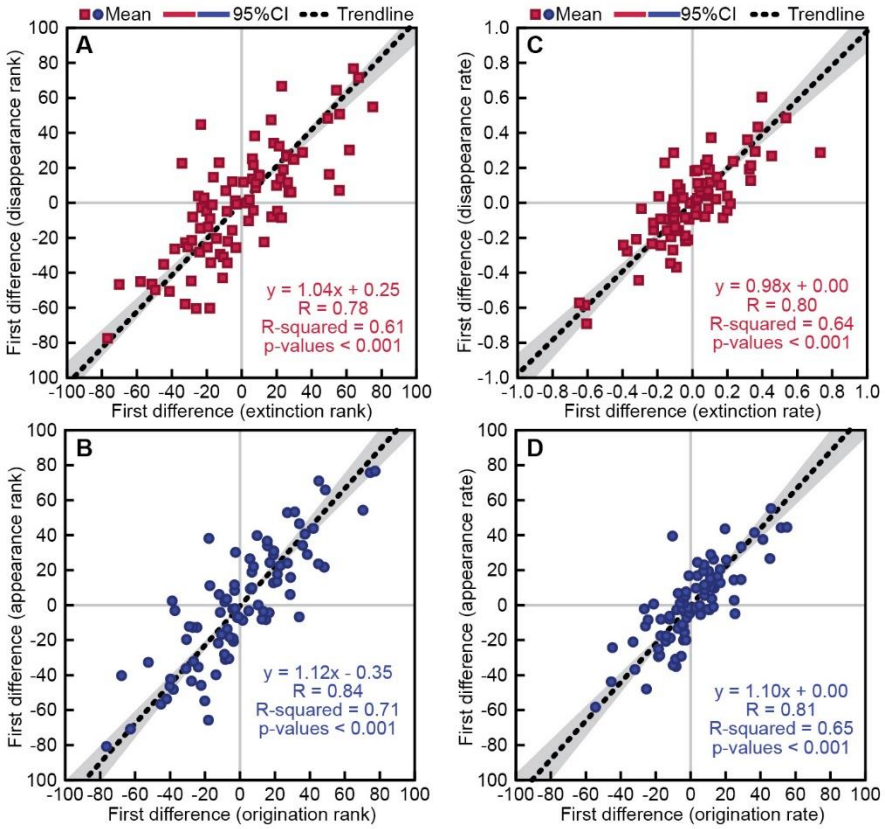

Figure S13. Correlations between first-differences of taxonomic and ecologic turnover. Each point (n=88) represents two consecutive time bins, and the axes are the differences (Figs. 3, S7, S9) between their turnover proportions (e.g., Figs. 2, S6C-E). Whereas (A, B) represent differences in ranked (ordinal) data, (C, D) represent differences in raw turnover proportions. A: Difference in rank of extinction proportion of marine and marginal marine animal genera (x-axis) versus difference in rank of the disappearance proportion of paleocommunities (y-axis). B: Difference in rank of the origination proportion of the taxa (x-axis) versus difference in the rank of the appearance proportion of the paleocommunities (y-axis). C: Difference in the extinction proportion of marine and marginal marine animal genera (x-axis) versus difference in the disappearance proportion of paleocommunities (y-axis). D: Difference in the origination proportion of the taxa (x-axis) versus difference in the appearance proportion of the paleocommunities (y-axis). Each plot includes a trendline from reduced major axis regression; coefficient of correlation (R value); coefficient of determination (R-squared value); and associated p-values. Correlations with p-values less than alpha (0.05) are statistically significant. The y-axis values are averages of best estimates from 200 runs of Infomap; and the x-axis values are averages from 1000 subsamples of SQS.

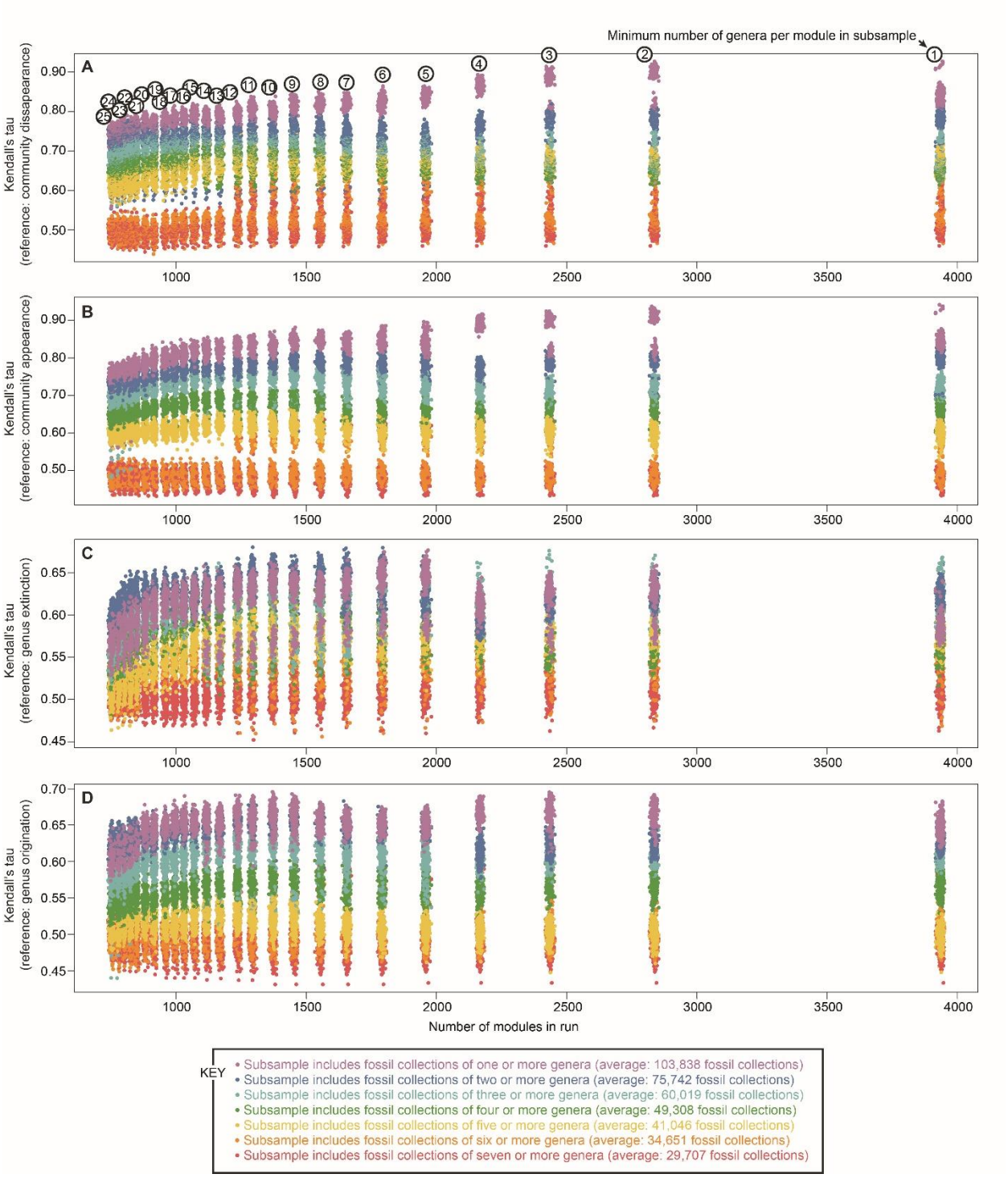
Minimum number of genera per module in subsample
A
B
C
D
Kendall's tau (reference: community dissapearance)
Kendall's tau (reference: community appearance)
Kendall's tau (reference: genus extinction)
Kendall's tau (reference: genus origination)
Number of modules in run
KEY
Subsample includes fossil collections of one or more genera (average: 103,838 fossil collections)
Subsample includes fossil collections of two or more genera (average: 75,742 fossil collections)
Subsample includes fossil collections of three or more genera (average: 60,019 fossil collections)
Subsample includes fossil collections of four or more genera (average: 49,308 fossil collections)
Subsample includes fossil collections of five or more genera (average: 41,046 fossil collections)
Subsample includes fossil collections of six or more genera (average: 34,651 fossil collections)
Subsample includes fossil collections of seven or more genera (average: 29,707 fossil collections)

Figure S14. Results of sensitivity analysis. Each point (n=36,400) represents a non-random subsample of collections and modules from one of the 200 runs of the Infomap Algorithm on the network in this study (Fig. S2). The analysis involved a four-step procedure. First, collections and modules were systematically excluded from each subsample at various thresholds related to the collections' and modules' numbers of genera. Then, the data were standardized using the SQS method using the subsample function of the divDyn package in R (Kocsis et al., 2019) and the smallest quorum size (usually between 0.7 and 0.9) that did not result in an error. This step involved 1000 iterations, and the results were adjusted with a sample coverage estimators based on single collection/occurrence modules (Alroy, 2010). Next, each subsample was used to calculate new paleocommunity (appearance and disappearance) turnover proportions. (Alroy, 2010). Finally, those proportions were compared to the references—the ecologic turnover proportions calculated from the whole network (Figs. 2, S6C, S6D) as well as the taxonomic turnover proportions of marine and marginal marine animal genera in the PBDB (Fig. S6E)—through calculation of rank correlation coefficients and associated p values. For all plots, the x-axis is the number of modules in the subsample, and y-axis is a Kendall rank correlation coefficient (τ). A: Subsampled versus whole network paleocommunity disappearance proportions. B: Subsampled versus whole network paleocommunity appearance proportions. C: Subsampled paleocommunity disappearance proportion versus genus extinction proportion. D: Subsampled paleocommunity appearance proportion versus genus origination proportion. The minimum number of genera per module in each subsample are shown in (A), and the collections' taxonomic richness thresholds are illustrated by the colors of the points. The average number of collections (minus those in excluded modules) is provided in the key for each threshold level of collection richness. For (A, B), the subsamples with highest τ values produced the paleocommunity turnover proportions that were most similar to those of the whole network (Fig. S2), and for (C, D), the best correlations between taxonomic and ecologic turnover have the highest τ values. All τ values are statistically significant (p values < 0.05).

Table S1. Paleoenvironments of fossil collections. The data were accessed from the Paleobiology Database (PBDB) and revised to reduce redundancy and overlap (indet. = indeterminate).

Paleoenvironment ('environment' in PBDB)	**Paleoenvironment (revised)**		**Paleoenvironment ('environment' in PBDB)**	**Paleoenvironment (revised)**
"channel"	fluvial/alluvial		lacustrine - large	lacustrine
"floodplain"	fluvial/alluvial		lacustrine - small	lacustrine
alluvial fan	fluvial/alluvial		lacustrine delta front	lacustrine
basin reef	reef		lacustrine delta plain	lacustrine
basinal (carbonate)	slope and basin		lacustrine deltaic indet.	lacustrine
basinal (siliceous)	slope and basin		lacustrine indet.	lacustrine
basinal (siliciclastic)	slope and basin		lagoonal	paralic
carbonate indet.	other or unknown		lagoonal/restricted shallow subtidal	paralic
cave	karst		levee	fluvial/alluvial
channel lag	fluvial/alluvial		loess	eolian
coarse channel fill	fluvial/alluvial		marginal marine indet.	other or unknown
coastal indet.	other or unknown		marine indet.	other or unknown
crater lake	lacustrine		mire/swamp	mire/swamp
crevasse splay	fluvial/alluvial		offshore	offshore shelf
deep subtidal indet.	deep subtidal		offshore indet.	offshore shelf
deep subtidal ramp	deep subtidal		offshore ramp	offshore shelf
deep subtidal shelf	deep subtidal		offshore shelf	offshore shelf
deep-water indet.	slope and basin		open shallow subtidal	shallow subtidal
delta front	deltaic		paralic indet.	paralic
delta plain	deltaic		perireef or subreef	reef
deltaic indet.	deltaic		peritidal	peritidal
dry floodplain	fluvial/alluvial		platform/shelf-margin reef	reef
dune	eolian		pond	lacustrine
eolian indet.	eolian		prodelta	deltaic
estuary/bay	paralic		reef, buildup or bioherm	reef
fine channel fill	fluvial/alluvial		sand shoal	shallow subtidal
fissure fill	karst		shallow subtidal indet.	shallow subtidal
fluvial indet.	fluvial/alluvial		shoreface	shallow subtidal
fluvial-deltaic indet.	fluvial/alluvial		sinkhole	karst
fluvial-lacustrine indet.	fluvial/alluvial		slope	slope and basin
foreshore	peritidal		slope/ramp reef	reef
glacial	glacial		spring	spring
glauconitic	other or unknown		submarine fan	slope and basin
interdistributary bay	paralic		tar	tar
interdune	eolian		terrestrial indet.	other or unknown
intrashelf/intraplatform reef	reef		transition zone/lower shoreface	deep subtidal
karst indet.	other or unknown		wet floodplain	fluvial/alluvial

Table S2. Lithologies of the rocks that yielded the fossil collections. The data were accessed from the Paleobiology Database (PBDB) and revised to reduce redundancy and overlap.

Lithology ('lithology1' in PBDB)	**Lithology (revised)**		**Lithology ('lithology1' in PBDB)**	**Lithology (revised)**
"carbonate"	not reported		gravel	gravel
"limestone"	not reported		ironstone	ironstone
"mixed carbonate-siliciclastic"	not reported		lignite	lignite
"reef rocks"	not reported		lime mudstone	lime mudstone
"shale"	not reported		marl	marl
"siliciclastic"	not reported		mudstone	mudstone
"volcaniclastic"	not reported		not reported	not reported
amber	amber		packstone	packstone
ash	ash		peat	peat
bafflestone	bafflestone		phosphorite	phosphorite
bindstone	bindstone		phyllite	phyllite
breccia	breccia		quartzite	quartzite
chalk	chalk		radiolarite	radiolarite
chert	chert		rudstone	rudstone
claystone	claystone		sandstone	sandstone
coal	coal		schist	schist
conglomerate	conglomerate		siderite	siderite
diatomite	diatomite		siltstone	siltstone
dolomite	dolomite		slate	slate
floatstone	floatstone		tar	tar
framestone	framestone		tuff	tuff
grainstone	grainstone		wackestone	wackestone

Table S3. Assortativity coefficients. Assortativity coefficients measure homophily, or the tendency of the nodes to connect to others possessing similar properties. Each row is a property of the fossil collections in the network, and values in parentheses are fields in the Paleobiology Database (PBDB). Assortativity coefficients were calculated for both nominal and continuous properties.

Node property	**Property type**	**Assortativity Coefficient**
Formation (‘formation’)	Nominal	0.07
Country (‘cc’)	Nominal	0.17
State (‘state’)	Nominal	0.13
Tectonic plate (‘geoplate’)	Nominal	0.18
Lithology (‘lithology1’)	Nominal	0.13
Lithology (revised from PBDB)	Nominal	0.12
Paleoenvironment (‘environmemt’)	Nominal	0.13
Paleoenvironment (revised from PBDB)	Nominal	0.15
Chronostratigraphic stage (‘time_major’)	Nominal	0.20
Chronostratigraphic system	Nominal	0.60
Maximum absolute age (‘max_ma’)	Continuous	0.96
Minimum absolute age (‘min_ma‘)	Continuous	0.96
Best age estimate: average of ‘max_ma’ & ‘min_ma’	Continuous	0.96
Taxonomic/generic richness	Continuous	0.10
Number of links to other collections	Continuous	0.35

Table S4. Results of different community detection algorithms. Five community detection algorithms were applied to the network (Csardi and Nepusz, 2006). In this analysis, each connection weight is a Jaccard coefficient. For the Infomap Algorithm, node weight equals taxonomic (generic) richness; in all other cases, the nodes are not weighted. These algorithms were selected because their computational complexity is relatively low (i.e., they ran to completion on the network on the order of minutes) and they do not require specification of additional parameters (e.g., step distance or cluster overlap). For each algorithm, the results include the number of modules (N) and modularity score (Q). The Louvain, fast greedy, and leading eigen algorithms are deterministic methods, meaning that their results do not vary from run to run (Csardi and Nepusz, 2006; Muscente et al., 2019; Muscente et al., 2018; Yang et al., 2016). In contrast, Infomap and Label Propagation algorithms are non-deterministic algorithms, and their results may vary from one run to the next (Csardi and Nepusz, 2006; Muscente et al., 2019; Muscente et al., 2018; Yang et al., 2016). To address this variation, we applied each of these algorithms 200 times to the network, and determined the average, minimum (min), and maximum (max) values of N and Q.

Algorithm	**Average N**	**Min N**	**Max N**	**Average Q**	**Min Q**	**Max Q**
Infomap	3937	3917	3951	0.85	0.85	0.85
Louvain	146	N/A	N/A	0.84	N/A	N/A
Fast Greedy	234	N/A	N/A	0.78	N/A	N/A
Leading Eigen	51	N/A	N/A	0.78	N/A	N/A
Label Propagation	3319	3262	3412	0.77	0.74	0.79

Table S5. Results of the Infomap Algorithm with different similarity coefficients. Four versions of the network were produced that differed with regard to connection weight. In this analysis, node weight equals taxonomic (generic) richness, and each connection weight is a similarity coefficient. The connection weights of the four versions of the network were calculated using the following indices: the Jaccard (Jaccard, 1901), Second Kulczynski (Kulczynski, 1928), Simpson (Simpson, 1960), and Sørensen–Dice (Dice, 1945; Sørensen, 1948) coefficients. For each version of the network, the Infomap Algorithm was applied 25 times, and the average, minimum (min), and maximum (max) numbers of modules (N) and modularity (Q) scores were determined.

Similarity index	**Average N**	**Min N**	**Max N**	**Average Q**	**Min Q**	**Max Q**
Jaccard	3937	3917	3951	0.85	0.85	0.85
Second Kulczynski	1767	1749	1784	0.75	0.75	0.76
Simpson	1223	1214	1233	0.73	0.72	0.73
Sørensen–Dice	2984	2975	2992	0.73	0.72	0.73

Table S6. Distance metrics comparing different runs of the Infomap Algorithm on the network. In this analysis, node weight equals taxonomic (generic) richness, and each connection weight is a Jaccard coefficient. A total of 200 runs of the algorithm were conducted on the network, and from these results, 100 pairs of community structures (sets of modules) were compared with four distance metrics, related to the similarity of the clusterings and their shared information (Csardi and Nepusz, 2006). In the case of normalized mutual information (NMI) and the Rand indices, values range from 0 to 1 and are measures of similarity (i.e., identical clusterings produce values equal to 1). Variation of information (VI), in contrast, measures dissimilarity (i.e., identical clusterings produce values equal to 0). The results include the average, minimum, and maximum values observed among the 100 calculations.

Distance Metric	**Average**	**Minimum**	**Maximum**
Normalized Mutual Information (NMI)	0.99	0.99	0.99
Variation of Information (VI)	0.15	0.12	0.19
Rand Index	1	1	1
Adjusted Rand Index	0.97	0.95	0.98

Table S7. Results of random forest analysis. A total of 200 runs of the Infomap Algorithm were conducted on the network, in which node weight equals taxonomic (generic) richness and each connection weight equals a Jaccard coefficient. Each run returned a community structure (set of modules). To each of these clusterings, we applied a random forest algorithm (Breiman, 2001), a method that involves permuting each variable, in order to compare the nodes' properties in terms of their importance as predicators of community structure (i.e., classification). The results include the average, minimum, and maximum values of importance, or the loss of function in mean squared error, measured using the Gini index ('IncNodePurity' in the randomForest function of the randomForest package in R).

Node Property	**Average**	**Minimum**	**Maximum**
Tectonic plate ('geoplate')	1.81E+09	1.74E+09	1.88E+09
Paleoenvironment (revised from PBDB)	1.05E+09	1.4E+09	1.48E+09
Lithology (revised from PBDB)	1.44E+09	1.02E+09	1.09E+09
Chronostratigraphic system	1.26E+09	1.22E+09	1.32E+09

Table S8. Results of standardization analysis. The nodes of the network in this study were repeatedly subsampled in order to produce 100 random subnetworks, which were analyzed with the Infomap Algorithm. In these analyses, node weight equals taxonomic (generic) richness, and each connection weight is a Jaccard coefficient. The results of each subnetwork analysis were compared to a random clustering from the full network using a number of distance metrics for comparing clusterings: NMI, VI, and the Rand and Adjusted Rand indices (Csardi and Nepusz, 2006). In addition, the number of collection (n), number of modules (N) and modularity (Q) of each subnetwork clustering was recorded. The results include the average, minimum, and maximum value among the 100 runs for each value. In the case of NMI and the Rand indices, values range from 0 to 1 and are measures of similarity (i.e., identical clusterings produce values equal to 1). In contrast, VI measures dissimilarity (i.e., identical clusterings produce values equal to 0).

Measurement	**Average**	**Minimum**	**Maximum**
Normalized Mutual Information (NMI)	0.95	0.94	0.95
Variation of Information (VI)	0.72	0.68	0.76
Rand Index	>0.99	>0.99	>0.99
Adjusted Rand Index	0.85	0.82	0.88
Number of collections (n)	50588.51	50472	50664
Number of modules (N)	2453.92	2402	2507
Modularity score (Q)	0.85	0.85	0.86

Data S1. (separate file)

An .xlsx file with the raw data and large tables produced by the analyses in this study is available for download from the Texas Data Repository at the following link (Muscente et al., 2021):

https://doi.org/10.18738/T8/NZFFME

Supplementary References

Alroy, J., 2003, Global database will yield reliable measures of global biodiversity: Paleobiology, v. 29, p. 26–29.

-, 2008, Dynamics of origination and extinction in the marine fossil record: Proceedings of the National Academy of Sciences, v. 105, no. 1, p. 11536–11542.

-, 2010, Fair sampling of taxonomic richness and unbiased estimation of origination and extinction rates, *in* Alroy, J., and Hunt, G., eds., Quantitative Methods in Paleobiology, Volume 16, The Paleontological Society Papers, p. 55–80.

-, 2015, A more precise speciation and extinction rate estimator: Paleobiology, v. 41, no. 4, p. 633–639.

Balseiro, D., and Powell, M. G., 2019, Carbonate collapse and the late Paleozoic ice age marine biodiversity crisis: Geology, v. 48, no. 2, p. 118–122.

Bambach, R. K., 2006, Phanerozoic biodiversity mass extinctions: Annual Review of Earth and Planetary Sciences, v. 34, no. 1, p. 127–155.

Bond, D. P. G., and Grasby, S. E., 2017, On the causes of mass extinctions: Palaeogeography, Palaeoclimatology, Palaeoecology, v. 478, no. Supplement C, p. 3–29.

Bowring, S. A., Erwin, D. H., and Isozaki, Y., 1999, The tempo of mass extinction and recovery: The end-Permian example: Proceedings of the National Academy of Sciences, v. 96, no. 16, p. 8827–8828.

Breiman, L., 2001, Random Forests: Machine Learning, v. 45, no. 1, p. 5–32.

Chen, Z.-Q., and Benton, M. J., 2012, The timing and pattern of biotic recovery following the end-Permian mass extinction: Nature Geoscience, v. 5, no. 6, p. 375–383.

Clauset, A., Newman, M. E. J., and Moore, C., 2004, Finding community structure in very large networks: Physical Review E, v. 70, no. 6, p. 1–6.

Csardi, G., and Nepusz, T., 2006, The igraph software package for complex network research: InterJournal Complex Systems, v. 1695, no. 5, p. 1–9.

Dice, L. R., 1945, Measures of the amount of ecologic association between species: Ecology, v. 26, p. 297–302.

Foster, W. J., Danise, S., Price, G. D., and Twitchett, R. J., 2017, Subsequent biotic crises delayed marine recovery following the late Permian mass extinction event in northern Italy: PLOS ONE, v. 12, no. 3, p. e0172321.

Foster, W. J., Garvie, C. L., Weiss, A. M., Muscente, A. D., Aberhan, M., Counts, J. W., and Martindale, R. C., 2020, Resilience of marine invertebrate communities during the early Cenozoic hyperthermals: Scientific Reports, v. 10, no. 1, p. 2176.

Jaccard, P., 1901, Distribution de la flore alpine dans le Bassin des Dranses et dans quelques regions voisines: Bulletin de la Société Vaudoise des Sciences Naturelles, v. 37, p. 241–272.

Karrer, B., Levina, E., and Newman, M. E. J., 2008, Robustness of community structure in networks: Physical Review E, v. 77, no. 4, p. 1–10.

Kocsis, Á. T., Reddin, C. J., Alroy, J., and Kiessling, W., 2019, The r package divDyn for quantifying diversity dynamics using fossil sampling data: Methods in Ecology and Evolution, v. 10, no. 5, p. 735–743.

Kouchinsky, A., Bengtson, S., Runnegar, B., Skovsted, C., Steiner, M., and Vendrasco, M., 2012, Chronology of early Cambrian biomineralization: Geological Magazine, v. 149, no. 02, p. 221–251.

Kulczynski, S., 1928, Zespoły roślin w Pieninach: Bulletin de l'Académie Polonaise des Sciences et des Lettres, v. 2, p. 57–203.
Landing, E., Geyer, G., Brasier, M. D., and Bowring, S. A., 2013, Cambrian Evolutionary Radiation: Context, correlation, and chronostratigraphy—Overcoming deficiencies of the first appearance datum (FAD) concept: Earth-Science Reviews, v. 123, p. 133–172.
Legendre, P., 2018, Model II Regression User's Guide: R Edition: Available as a vignette of the R package lmodel2, p. 1–14.
McGhee, G. R., Clapham, M. E., Sheehan, P. M., Bottjer, D. J., and Droser, M. L., 2013, A new ecological-severity ranking of major Phanerozoic biodiversity crises: Palaeogeography, Palaeoclimatology, Palaeoecology, v. 370, p. 260–270.
McGhee, G. R., Sheehan, P. M., Bottjer, D. J., and Droser, M. L., 2012, Ecological ranking of Phanerozoic biodiversity crises: The Serpukhovian (early Carboniferous) crisis had a greater ecological impact than the end-Ordovician: Geology, v. 40, no. 2, p. 147–150.
Mukaka, M. M., 2012, A guide to appropriate use of correlation coefficient in medical research: Malawi Medical Journal, v. 24, no. 3, p. 69–71.
Muscente, A. D., Bykova, N., Boag, T. H., Buatois, L. A., Mángano, M. G., Eleish, A., Prabhu, A., Pan, F., Meyer, M. B., Schiffbauer, J. D., Fox, P., Hazen, R. M., and Knoll, A. H., 2019, Ediacaran biozones identified with network analysis provide evidence for pulsed extinctions of early complex life: Nature Communications, v. 10, no. 1, p. 1–15.
Muscente, A. D., Martindale, R. C., Prabhu, A., Ma, X., Fox, P., Hazen, R. M., and Knoll, A. H., 2021, Supplementary Data for ‘appearance and disappearance rates of Phanerozoic marine animal paleocommunities:’ Texas Data Repository, V1, https://doi.org/10.18738/T8/NZFFME
Muscente, A. D., Prabhu, A., Zhong, H., Eleish, A., Meyer, M. B., Fox, P., Hazen, R. M., and Knoll, A. H., 2018, Quantifying ecological impacts of mass extinctions with network analysis of fossil communities: Proceedings of the National Academy of Sciences, v. 115, no. 20, p. 5217–5222.
Peters, S. E., and McClennen, M., 2015, The Paleobiology Database application programming interface: Paleobiology, v. 42, no. 1, p. 1–7.
Powell, M. G., 2008, Timing and Selectivity of the Late Mississippian Mass Extinction of Brachiopod Genera from the Central Appalachian Basin: PALAIOS, v. 23, no. 7/8, p. 525–534.
Raup, D. M., and Sepkoski, J. J., Jr, 1982, Mass extinctions in the marine fossil record: Science, v. 215, p. 1501–1503.
Rosvall, M., Axelsson, D., and Bergstrom, C. T., 2010, The map equation: The European Physical Journal Special Topics, v. 178, p. 13–23.
Rosvall, M., and Bergstrom, C. T., 2007, An information-theoretic framework for resolving community structure in complex networks: Proceedings of the National Academy of Sciences, v. 104, no. 18, p. 7327–7331.
Schober, P., Boer, C., and Schwarte, L. A., 2018, Correlation coefficient: Appropriate use and interpretation: Anesthesia & Analgesia, v. 126, no. 5, p. 1763–1768.
Sepkoski, J. J., 1982, Mass extinctions in the Phanerozoic oceans: A review: Geological Society of America Special Paper, v. 190, p. 283–289.
Servais, T., and Harper, D. A. T., 2018, The Great Ordovician Biodiversification Event (GOBE): definition, concept and duration: Lethaia, v. 51, no. 2, p. 151–164.

Servais, T., Lehnert, O., Li, J., Mullins, G. L., Munnecke, A., Nützel, A., and Vecoli, M., 2008, The Ordovician Biodiversification: Revolution in the oceanic trophic chain: Lethaia, v. 41, p. 99–109.
Sheehan, P. M., 1996, A new look at Ecologic Evolutionary Units (EEUs): Palaeogeography, Palaeoclimatology, Palaeoecology, v. 127, no. 1, p. 21–32.
Shi, G. R., 1993, Multivariate data analysis in palaeoecology and palaeobiogeography—a review: Palaeogeography, Palaeoclimatology, Palaeoecology, v. 105, no. 3, p. 199–234.
Simpson, G. G., 1960, Notes on the measurement of faunal resemblance: American Journal of Science, v. 258, p. 300–311.
Smith, R. J., 2009, Use and misuse of the reduced major axis for line-fitting: American Journal of Physical Anthropology, v. 140, no. 3, p. 476–486.
Sørensen, T., 1948, A method of establishing groups of equal amplitude in plant sociology based on similarity of species and its application to analysis of the vegetation on Danish commons: Kongelige Danske Videnskabernes Selskab, v. 5, p. 1–34.
Speijer, R. P., Scheibner, C., Stassen, P., and Abdel-Mohsen, M. M., 2012, Response of marine ecosystems to deep-time global warming: A synthesis of biotic patterns across the Paleocene-Eocene thermal maximum (PETM): Australian Journal of Earth Sciences, v. 105, no. 1, p. 6–16.
Takashima, R., Nishi, H., Huber, B. T., and Leckie, R. M., 2006, Greenhouse world and the Mesozoic ocean: Oceanography, v. 19, no. 4, p. 82–92.
Webby, B. D., 2004, The Great Ordovician Biodiversification Event, New York, Columbia University Press, 484 p.
Yang, Z., Algesheimer, R., and Tessone, C. J., 2016, A comparative analysis of community detection algorithms on artificial networks, v. 6, p. 30750.